# Report on

# Open RDA – RVP8 Signal Processing

# Part 1 – Simulation Study

Including

Gaussian Model Adaptive Processing (GMAP)

Clutter Filter Evaluation


Prepared by

Richard L. Ice, RS Information Systems

David A. Warde and Dale Sirmans, Systems Technology Associates

Darrel Rachel, Management and Engineering Technology International

WSR-88D Radar Operations Center
Engineering Branch

Norman, Oklahoma



January 2004

Table of Contents

# List of Figures

# List of Tables

## 1. Executive Summary

This report covers results of a Radar Operations Center (ROC) tasking which validates signal processing performance of the Open Radar Data Acquisition (ORDA) System. The ROC is responsible for ensuring that ORDA signal processing, including base moment estimators and clutter filters, meets NEXRAD program functional requirements. This analysis includes evaluations of all base moments and the new Gaussian Model Adaptive Processing (GMAP) clutter signal management technique developed at SIGMET.

The ROC team uses several evaluation methods for verifying performance. Engineers use a digital signal simulation utility to characterize the signal processor algorithms, initially focusing on spectrum width. The spectrum width estimators are of interest because the ORDA allows use of the poly-pulse or lag 2-covariance estimator in addition to the basic estimator deployed with the WSR-88D. This evaluation project addresses performance differences in the two estimators and reviews ORDA design and selection criteria. The commercial signal processor supplier, SIGMET, Inc., provided improvements to the spectrum width estimators and clutter filters during the project and the resultant versions of software are also evaluated in this report.

The analysis is conducted with a variety of weather parameters, including selected ranges of signal powers, mean velocities, and mean spectrum widths.

Major conclusions are:

- Both the R0/R1 (with noise compensation) and R1/R2 spectrum width estimators meet WSR-88D benchmark requirements. The R0/R1 estimator delivers a lower

variance of estimate over a larger spectrum width range but requires system noise compensation. The R1/R2 estimator is immune to system noise but delivers quality estimates over about one-half the spectrum width range of R0/R1.

- The GMAP method of clutter suppression and spectral restoration meets most of the WSR-88D benchmark requirements. Standard deviation of velocity estimates are larger than specified (< 2 $ms^{-1}$) at small number of samples and large clutter to signal ratios. Reflectivity and spectrum width bias and standard deviation are compliant with specifications (reflectivity bias and standard deviation < 2 dB, velocity moment bias and standard deviation < 2 $ms^{-1}$).

- Maximum clutter suppression is about 55 dB (Clutter to Signal Ratio, as compared to 55 dB Clutter to Noise Ratio for the legacy) and the technique recovers signals on and near the zero isotach with small bias and little signal distortion as opposed to the large bias and distortion of the legacy filter.

- GMAP with the Blackman window exhibits significantly better performance than with the Hamming window. The Adaptive window option in the present state of development does not offer any advantage over the choice of the Blackman window.

- Performance of the GMAP filter depends on matching filter width to expected clutter spectrum width. If the widths cannot be matched accurately, then the GMAP filter width should be wider than the expected range of clutter widths.

- The evaluation team concludes that the RVP8 reflectivity, velocity and R1/R2 spectrum width moment estimators meet WSR-88D performance requirements. The noise compensated R0/R1 spectrum width estimator also meets requirements. The team concludes that the GMAP clutter management techniques meet WSR-88D requirements also.

Major recommendations are:

- Use of the GMAP clutter filtering technique in the ORDA.

- Development of a new clutter map generation scheme to include spectrum width measurements necessary for the GMAP technique.

- Retention of both the R0/R1 and R1/R2 spectrum width estimators and development of an adaptive spectrum width estimator selection process.

- Development of enhanced radar system noise measurement quality control methods.

- If only one spectrum width estimator is selected initially, it should be the R0/R1 noise compensated version.

- Improvements to the Adaptive window selection technique should be a part of future RDA enhancements.

In addition to simulations covered in this report, the engineering team will incorporate real radar data in a subsequent study. This will include a limited amount of time series data previously archived. The ROC team has access to a number of time series data sets recorded from a similar radar system, specifically the NCAR S-Pol research radar. In this second phase, the engineering team will pay particular attention to differences such as increased variance and estimator bias.

## 2. Introduction and Background

The WSR-88D Radar Operations Center (ROC) is evaluating the new signal processor, digital receiver, and software algorithms under development by the National Weather Service (NWS) Office of Science and Technology (OST), Open Radar Data Acquisition (ORDA) project (Cate, 2003). The ROC is responsible for ensuring that ORDA systems comply with WSR-88D system specifications, and is focusing on the performance of system signal processing algorithms, including base moment estimators and clutter filters. Radar Operations Center engineering team members are also evaluating the capability of the ORDA system to incorporate planned enhancements. These improvements include production of higher resolution base products, range-velocity ambiguity mitigation, range over sampling, and full power spectrum analysis. Another potential improvement which should integrate well with the RVP8 spectral processing capacity is the anomalously propagated clutter mitigation (featuring automatic clutter recognition) technique.

The initial focus is on performance of the basic moment estimators. The spectrum width estimation process is of particular interest because the SIGMET RVP8 system offers use of the poly-pulse, or R1/R2 estimator in addition to the traditional method currently employed in the WSR-88D. The ORDA system will likely make use of an optimal combination of both estimators, therefore it is important to fully characterize the performance of both.

The Open RDA team also asked ROC engineers to evaluate a new clutter filtering technique provided by SIGMET as a potential alternative to the legacy 5-pole elliptic time domain filter. This technique, designated as Gaussian Model Adaptive Processing

(GMAP) by SIGMET, is based on frequency domain processing in lieu of the traditional time domain process of the legacy elliptic filter. This report covers results of the base moment evaluation as well as the GMAP testing.

This report covers analysis methods available to the engineering team and reports results of the basic moment performance evaluation. The document includes an extended discussion of the GMAP technique and presents detailed performance results. Discussions include a review of WSR-88D performance requirements in relevant areas.

During the course of the evaluation, the ROC engineering team provided interim results to both the ORDA team as well as SIGMET. As a result of this feedback, SIGMET modified the RVP8 software to correct performance issues noted during the simulations. The engineering team identified two major issues with algorithm performance. The first item noted was that the R0/R1 spectrum width estimator did not meet specifications for cases with low signal to noise ratios. This was expected since the original version of this estimator did not include compensation for system noise. The second issue was that the GMAP clutter filter algorithm performance did not meet specifications for cases with a low number of samples. Specifically, in modes where less than 32 samples were available, estimator bias and standard deviations were unacceptably high.

SIGMET provided two additional software releases to address these issues. The first one, release 8.04, changed the method GMAP uses for determining the system noise level. Release 8.04 makes use of a supplied system noise value rather than estimating the noise from signal characteristics using a rank order technique. This modification addressed the issue of GMAP performance at low numbers of samples. The second new

release (8.04.03) included noise compensation for the R0/R1 spectrum width estimator. This change resulted in the R0/R1 estimator performing within WSR-88D specifications.

With each new software release, the engineering team conducted relevant simulations and analysis to verify algorithm performance and to ensure no new issues were introduced. This report includes results from all three versions of the RVP8 software.

## 3. Summary of Analysis Methods

The evaluation is focused primarily on simulations, generating time series data with pre-determined characteristics as a controlled input to the RVP8 signal processor. Time series data with known mean values for signal power, velocity, and spectrum width provide a quantitative approach for characterizing performance of the signal processor. SIGMET provides a utility which is sufficient for this purpose. The A-scope digital signal simulator generates time series data based on user input via a graphical user interface. Operators can specify weather signal, noise, and clutter signal power levels, thereby establishing the signal to noise ratio (SNR) and clutter to signal ratio (CSR) for each of two independent weather signals. The operator can also specify the mean values of weather signal velocity and spectrum width as well as the spectrum width of the clutter signal. The digital signal simulator is an integrated utility provided with SIGMET's IRIS software package. This simulator is based on techniques used by early investigators researching velocity and spectrum width estimators [1]. The simulator generates weather and clutter spectra based on specified parameters and then produces time series data by means of an inverse Discrete Fourier Transform.

The A-scope signal simulator starts each simulation run with a randomly generated seed value. From this value, the software generates an array of 16,000 time series data points. For each ray or "trial" of data, the simulator picks a different starting point within this array of time series data and attempts to avoid overlaps. The data is designed to have a Gaussian distribution exhibiting the appropriate means and standard deviations associated with the specified weather, clutter, and noise signals.

The following plot (Figure 1) displays the Gaussian distribution of the simulated signals, done as a verification of simulator performance. This is the average of power spectral densities from 128 generated spectra, using 128 point transforms. The mean signal velocity is zero, the mean SNR is 30 dB and the spectrum width is 3 $ms^{-1}$. For this set of data the PRF is set for a Nyquist velocity of 25 $ms^{-1}$. This data is generated using a rectangular window for best spectral resolution and so that spectral broadening is minimized.

The result is plotted, and overlaid with an ideal Gaussian distribution with the same statistics. The data falls within an expected Gaussian distribution, but there are several areas where the curve does not fill in completely. Additional runs result in plots with similar characteristics, but with the missing areas on different points of the plot. The evaluation team concludes this characteristic is a result of the finite number of time series data elements generated for the array. With 16,000 values generated, with subsets selected for the simulation, and with a large number of trials from the set, some reuse of data takes place resulting in the apparent missing elements. This artifact does not affect the overall accuracy of the simulation since the team collects many data sets for each area of investigation and the overall characteristics are sufficiently Gaussian.

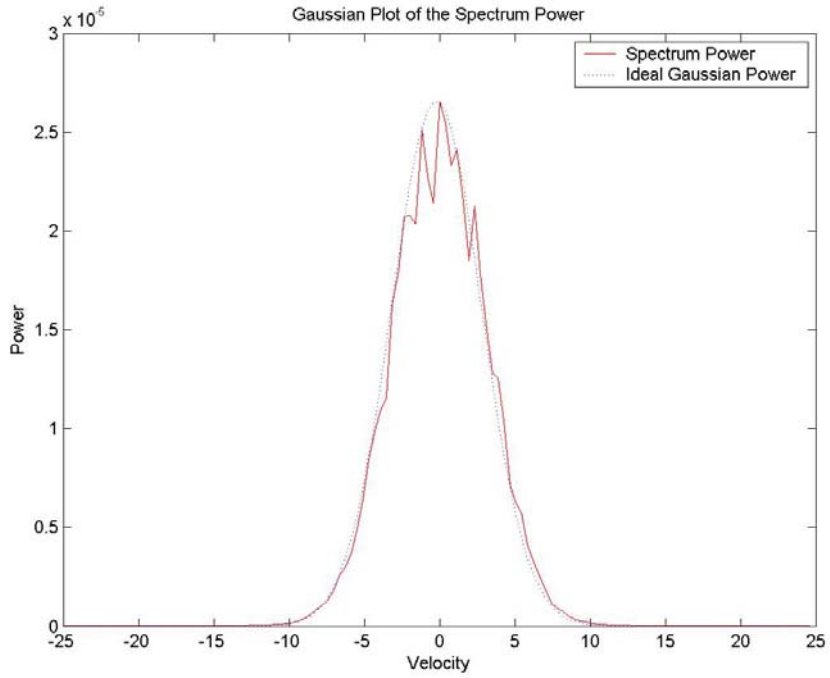


**Figure 1 - Gaussian Performance of A-scope Simulator (Example Run)**

The simulation runs are designed to encompass expected system performance parameters sufficient to verify requirements are met. Parameters are selected to cover all modes of WSR-88D operation. These modes include severe weather surveillance (long PRT with a low number of samples), severe weather Doppler (short PRT with moderate number of samples) and clear air mode (long PRT with large number of samples). In order to cover all modes, simulations use estimator sample sizes set for N = 16, 32, and 64 for most scenarios.

In order to cover WSR-88D modes, simulations are conducted for PRF's of 322, 450 and 1000 Hz. This corresponds to PRF 1, 2 and 5 for the severe weather surveillance, Doppler , and clear air modes. Simulations cover the full Nyquist velocity ranges for each of the PRF's selected. Spectrum width values of 0.5 to 8.0 $ms^{-1}$ are also

included. Generally, signal to noise values are set for a wide range of performance. Typically simulations included a SNR values from 10 dB to 50 dB.

Table 1 shows the set up parameters for the initial validations of the spectrum width estimators. The first simulations are using the initially available version of the RVP8 software (release 8.0). For this task, clutter and noise are both set at –80 dBm. All runs are were done with 5 signal levels, 7 velocities, and 5 widths as seen in the table. All runs are also completed for both of the available spectrum width estimators, the R0/R1 and R1/R2 estimators. Thus a total of 350 recordings is needed to encompass all simulation variables for this one area of investigation. Each recording contains 4,000 range bins with estimates for reflectivity, velocity and spectrum width along with a variable number of time series and spectrum plot data sets.

Table 1 - Simulator Parameters for Spectrum Width Estimator Evaluation

| | | | | | | | | | |
|---|---|---|---|---|---|---|---|---|---|
| Simulator Set-up | Signal (dBm) | -70 | -60 | -50 | -40 | -20 | | | 5 |
| | Velocity $V/V_n$ | -0.8 | -0.6 | -0.4 | 0 | 0.4 | 0.6 | 0.8 | 7 |
| | Width $W/V_n$ | 0.02 | 0.08 | 0.16 | 0.24 | 0.32 | | | 5 |
| | Clutter (dBm) | -80 | | | | | | | |
| | Noise (dBm) | -80 | | | | | | | |
| Processor Set-up | R0/R1 or R1/R2 | 1 | 1 | | | | | | 2 |
| | | | | | | | | | 350 Samples |

For each simulation set up, a total of 4,000 estimates are obtained. This is done by recording 400 bins per ray for each of ten rays. Since all range bins contain the same weather parameters in the simulation, all range bins are included in the evaluation. Recording is done with the A-scope recorder. Parameters recorded include filtered and unfiltered reflectivity, velocity, spectrum width, spectrum magnitude, and time series data. Spectrum magnitude and the time series data are classified as bin plots by SIGMET

and the operator must separately specify the number of these bins to record. Typically 20 bins are recorded unless the focus is on these particular outputs.

The data is recorded to files in the RVP8 native format. A MATLAB based conversion routine is used to convert the native format to real values and also to prepare the data for further analysis. The conversion routine reads the native values into the MATLAB workspace and converts the data based on format descriptions found in the RVP8 User's manual, under the definition of the "PROC" command. Once reflectivity, velocity, and spectrum width data sets are available, the overall statistics of the data set are computed and analyzed. Typically, the means of the large data sets are computed and imported into a Microsoft Excel spreadsheet for plotting.

A typical Excel plot of performance of the R0/R1 spectrum width estimator is shown in Figure 2.

This figure plots the mean of the calculated spectrum widths versus the mean spectrum widths set by the input simulation parameters. This data is for the original R0/R1 estimator supplied by SIGMET which does not employ noise compensation. The effect of this is seen as a bias in the curves related to lower signal to noise values (below 30 dB).

Another measure of estimator performance is the standard deviation of the output data sets. Figure 3 is a typical plot of estimator output standard deviation.

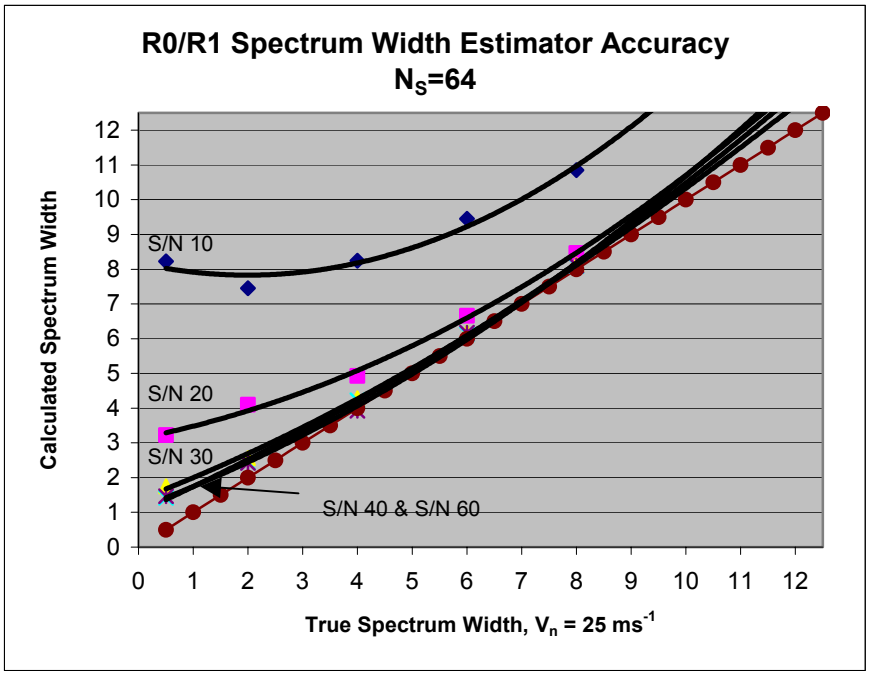


**Figure 2 - Bias Performance of the R0/R1 estimator (without noise compensation)**

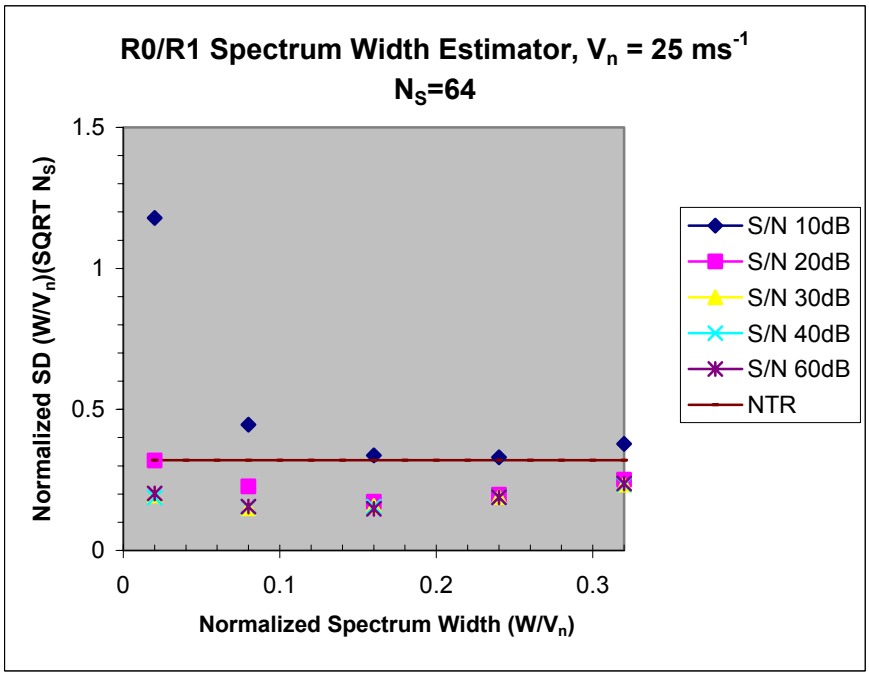


**Figure 3 - Standard Deviation of the R0/R1 Estimator (without noise compensation)**

Figure 3 shows the standard deviation of the output data as a function of input spectrum width and signal to noise ratio for the R0/R1 estimator. The X axis is normalized to the Nyquist velocity ($W/V_n$) where 'W' is spectrum width and $V_n$ is the Nyquist velocity. The Y axis is normalized using the Nyquist velocity and number of samples in a manner similar to that given in [6], that is $SD[W]N = \sqrt{N_S} * SD[W]/V_n$ , where $N_S$ is the number of samples in the estimate. WSR-88D requirements for width standard deviation are such that the deviation be less than 1 $ms^{-1}$ at an input width of 4 $ms^{-1}$ and a signal to noise ratio of 10 dB [2]. For the parameters associated with this data set, the 1 $ms^{-1}$ point is 0.32 on the Y axis and the line marked "NTR" denotes this value.

An approximation for the standard deviation of the R0/R1 estimator is provided in [9]. For low SNR the standard deviation is given by

$$SD[W] = 2V_a \left[ \frac{3}{32\pi^4} \frac{1}{m} \frac{N^2}{S^2} \right]^{1/2} \left( \frac{w}{2V_a} \right)$$

A plot of the standard deviation at low SNR is given in Figure 4.

From the equation and Figure 4, one can see that the deviation is linearly related to the spectrum width and increases as the signal to noise ratio decreases. For the WSR-88D specification parameters of w = 4 $ms^{-1}$ and SNR = 10 dB, the expected value of the width standard deviation is around 1 $ms^{-1}$ which is consistent with requirements.

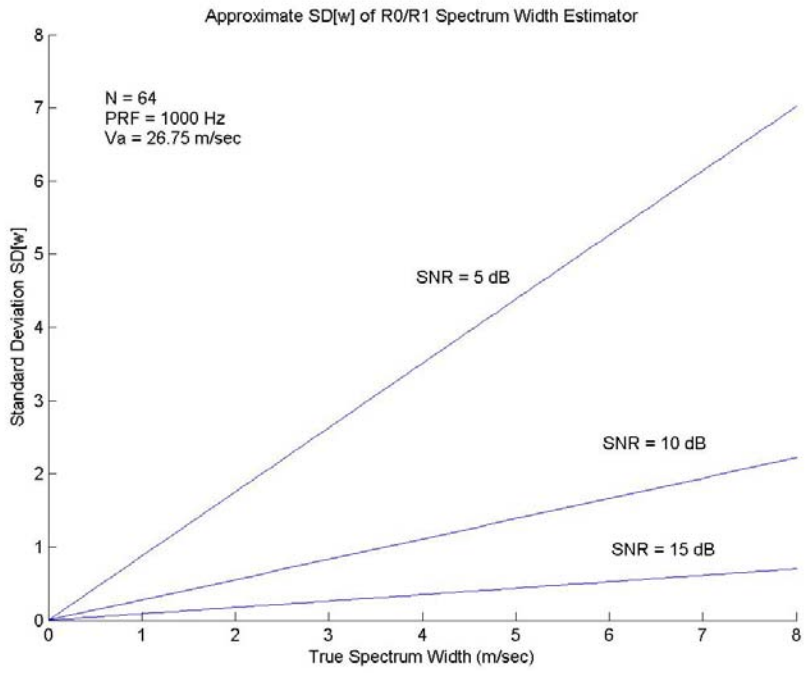


**Figure 4 - Approximate SD of R0/R1Estimator - Low SNR**

For high SNR, the standard deviation is given by:

$$SD[W] = 2V_a\left[\frac{3}{32\pi^4}\frac{1}{m}\right]^{1/2}\left(\frac{w}{2V_a}\right)^{1/2}$$

Figure 5 is a plot of this equation for the parameters associated with the convective mode VCP's (11 and 21).

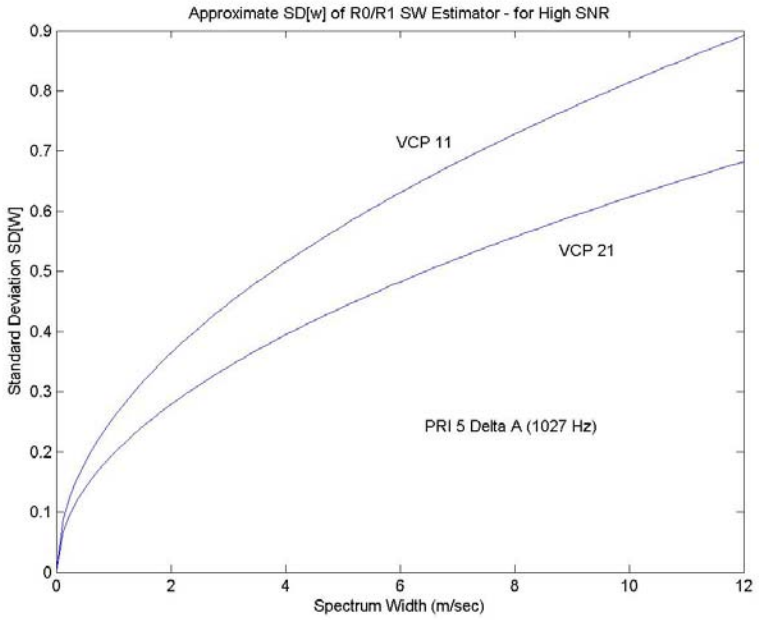


**Figure 5 - Approximate Standard Deviation of R0/R1 Estimator (High SNR)**

The equations used to generate the data of Figures 4 and 5 are approximations only, and don't cover every condition encountered in actual radar operations. They serve as a means to discern large scale behavior of the estimator however. That is, performance is better with higher signal to noise ratios. Also for sufficient signal to noise ratio (greater than 20 dB), the estimator performs better for broad spectrum widths as evidenced by the decreasing slope of the standard deviation plot of Figure 5 with increasing spectrum width.

The data can also be examined in detail through the use of histograms. These are plots of the distribution of estimator output values and are useful for examining statistical performance of a large set of samples. A typical histogram plot generated by a MATLAB routine is shown in Figure 6.

The histogram shows the number of estimates associated with each value of either spectrum width or velocity, i.e. the estimator outputs are sorted as a function of output

value with the vertical axis depicting the number of "hits" at each value. By examining the histogram, the mean value of the data set and the approximate standard deviation can be seen. In this example the input spectrum width is 4 $ms^{-1}$ and the input velocity is 8 meters per second. For the velocity plot, the data can be seen to be clustered around 8 $ms^{-1}$ as expected. However the width exhibits a slightly positive bias for this data set.

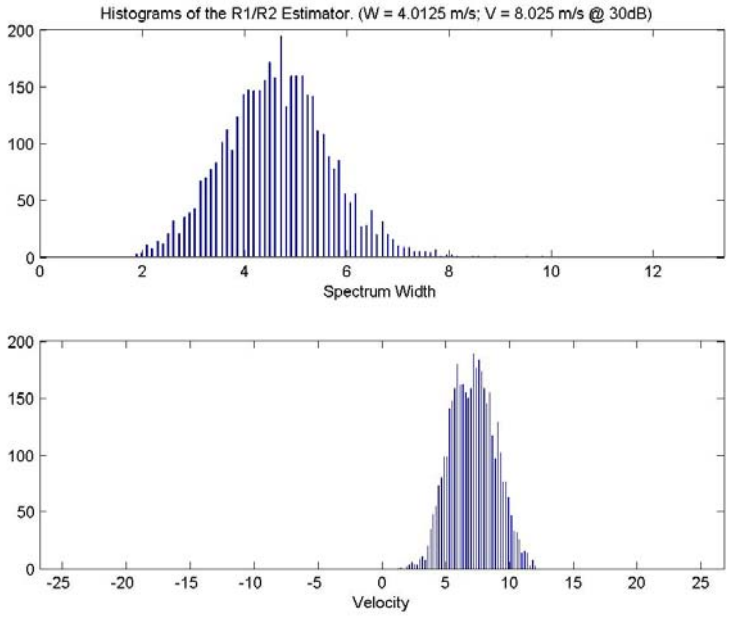


**Figure 6 - Typical Histogram Plot**

The histograms are also useful for observing behavior of the estimators under various conditions. For example, folding can be seen easily in a histogram for cases of large widths and high positive velocities.

Figure 7 depicts a number of attributes of the estimator output. With a spectrum width of 4 $ms^{-1}$ and a mean velocity of 24 $ms^{-1}$, some of the velocity estimator outputs are aliased into the negative Nyquist interval. This particular plot results from processing with a clutter signal and a clutter filter invoked. This output is from a simulation run

which was part of the GMAP evaluation described later. Some residue from the clutter filtering process is seen represented by the outputs clustered about the zero mean value. The distribution of the spectrum width outputs contains a large number of outputs at the minimum value of 0.01 $ms^{-1}$.

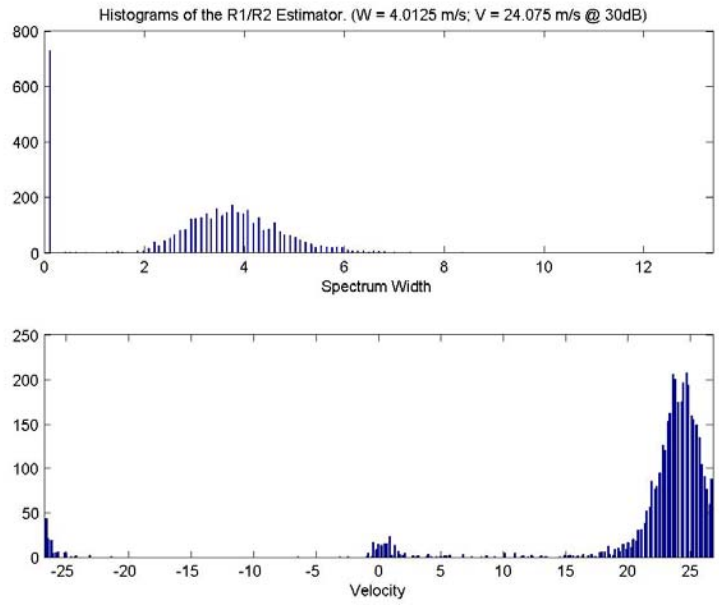


**Figure 7 - Histogram Plot Showing Velocity Folding**

The team also uses MATLAB to visualize the power spectrum of selected data sets. In Figure 8, an example of a three dimensional plot of 200 power spectra can be seen.

The simulation associated with this plot contains a clutter signal which is then processed through the SIGMET GMAP clutter filter. A small amount of clutter residue is seen along the zero velocity line, the signal power dominates and is centered along the expected 13.4 $ms^{-1}$ line.

All data, including basic ASCII files from the A-scope recorder, MATLAB converted data files, and Excel spreadsheets, are recorded on a Local Area Network

(LAN) drive contained within the ROC network so all team members can access the extensive data base.

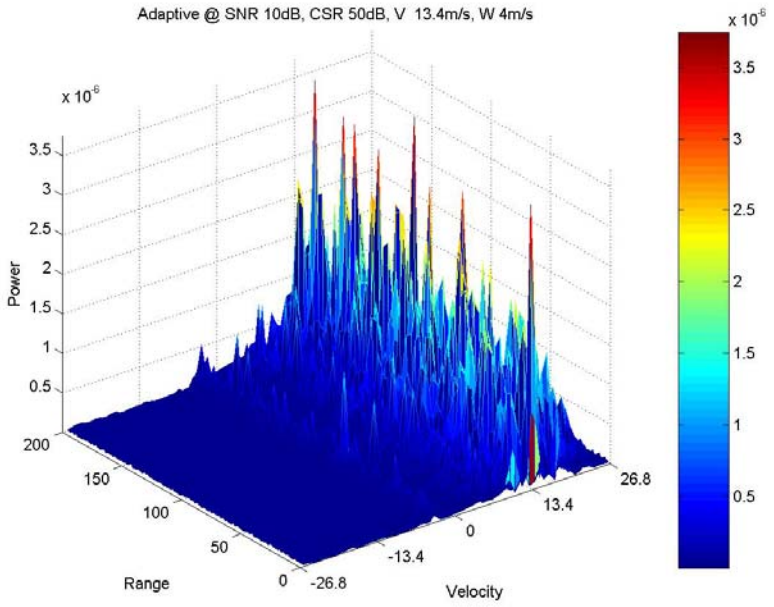


**Figure 8 - Example Power Spectrum Plots**

## 4. Spectrum Width Estimator Evaluation

Initial simulations and analysis focus on performance of the spectrum width estimators. This section addresses performance of the two spectrum width estimators without application of clutter filtering as this was the original focus of the study. This comparison of the two estimators is important as an input to ORDA system operation, architecture, and software design. Note that verification of the reflectivity and velocity estimators was not done separately, but is included in the section on GMAP performance. The first runs are with the original versions of the estimators which do not incorporate noise compensation. The results of not compensating for noise are most evident in the R0/R1 data shown previously in Figures 2 and 3 as the performance of that estimator is sensitive to noise contaminations. For Figure 2, the bias is seen to be excessive for signal

to noise ratios less than about 30 dB. Figure 3 is the standard deviation performance. As stated earlier, WSR-88D requirements for width standard deviation are such that the deviation be less than 1 $ms^{-1}$ at an input width of 4 $ms^{-1}$ and a signal to noise ratio of 10 dB. On the normalized X axis of Figure 3, the 4 $ms^{-1}$ point equates to a value of 0.16. It can be seen from the standard deviation graph in Figure 3 that the 4 $ms^{-1}$ point has a value just slightly above the NTR line. This version of the spectrum width estimator is just short of compliance with the WSR-88D standard deviation specification. Returning to the theoretical performance of Figures 4 and 5, it can be seen that the performance of the R0/R1 estimator follow the general trends expected.

Simulation set up parameters for this initial phase are as given in Table 1 in the previous section. Data for the R1/R2 (or "lag 2") estimator is now presented. Figure 9 shows bias performance of the R1/R2 estimator as a function of signal to noise ratio.

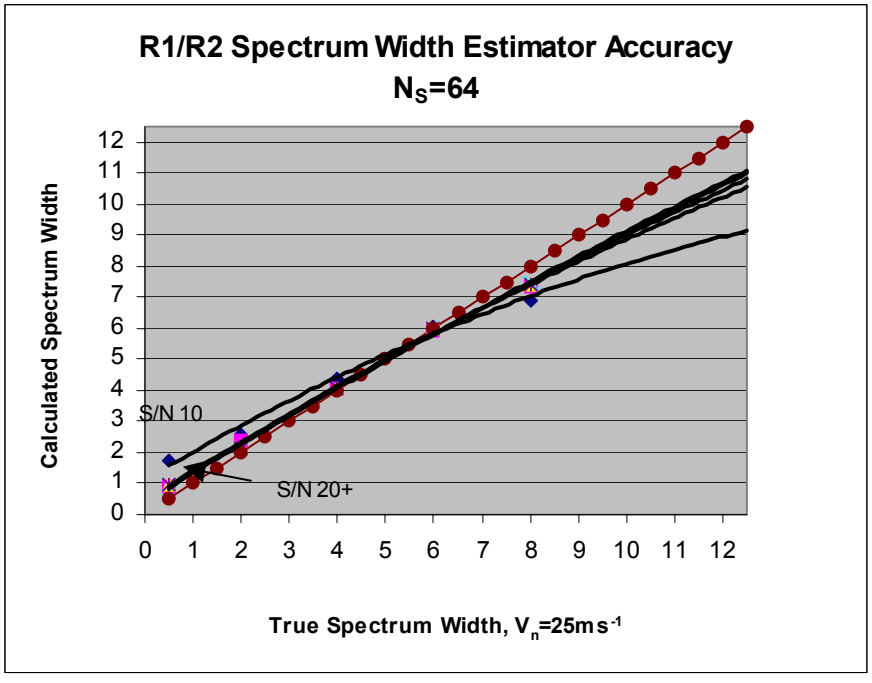


**Figure 9 - Bias Performance for R1/R2 Estimator**

Figure 10 shows the standard deviation of estimator outputs as a function of signal to noise ratio (SNR). This data is obtained in the same manner as for the R0/R1 estimators in the previous section. Scales are normalized as before with the NTR compliance line indicated. For the required width of 4 $ms^{-1}$ (0.16 on the X axis scale) it can be seen that this version of the width estimator is compliant with WSR-88D specifications (SD[W] less than 1$ms^{-1}$ at 10 dB SNR and 4 $ms^{-1}$ true width).

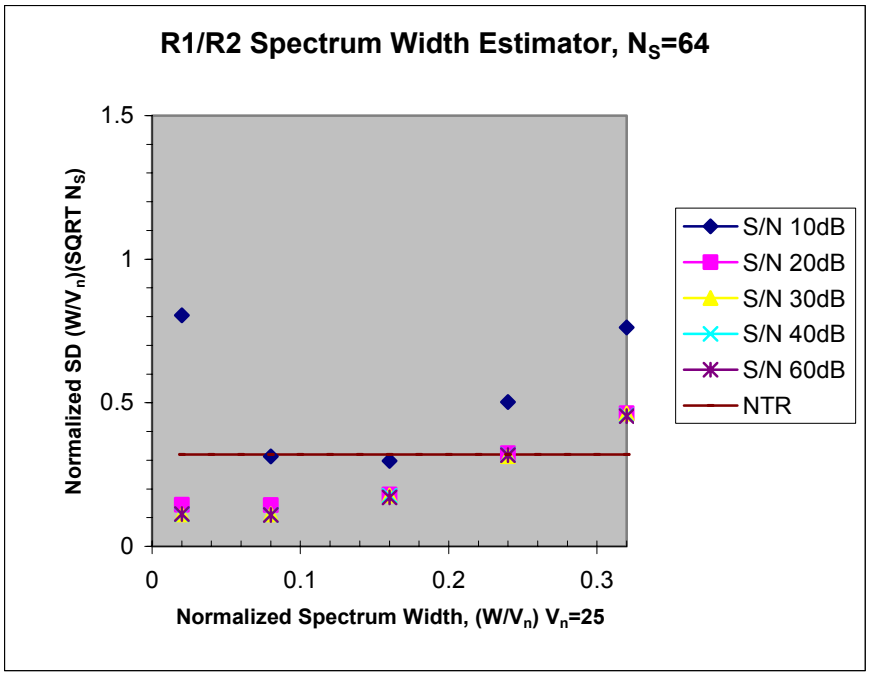


**Figure 10 - Standard Deviation of the R1/R2 Estimator**

A note on system noise estimation and handling is in order. The basic R0/R1 estimator did not initially compensate for noise, a significant difference from the way the WSR-88D estimator works. This issue results in the poor performance of the R0/R1 estimator seen in Figures 2 and 3 for low signal to noise ratios. The ORDA team tasked SIGMET to incorporate noise compensation. Also, during the course of the GMAP filter

evaluations, the ROC engineering team notified the ORDA group and SIGMET that the GMAP process did not meet specifications for the surveillance mode. SIGMET provided two additional software builds to address these issues. Build 8.04 addressed the issue with GMAP while Build 8.04.03 addressed the noise compensation issue. The ROC engineering team tested all moment estimators for all software builds. The results of additional spectrum width testing are presented in the next two sections while all GMAP test results are presented later. Simulations obtained for the spectrum width estimators using release 8.04 are documented in the next section.

## 5. Estimator Evaluation with System Noise Input (Release 8.04)

Table 2 displays the input parameters for the simulations related to Release 8.04 which makes use of supplied system noise instead of the estimated values.

Table 2 - Set Up For Incorporated System Noise Trials

| | | | | | | | |
|---|---|---|---|---|---|---|---|
| Simulator Set-up | Signal (dBm) | -70 | -60 | -50 | -40 | | 4 |
| | Velocity ($V/V_n$) | 0 | 0.4 | 0.6 | 0.8 | | 4 |
| | Width ($W/V_n$) | 0.02 | 0.08 | 0.16 | 0.24 | 0.32 | 5 |
| | Clutter (dBm) | --- | | | | | |
| | Noise (dBm) | -80 | | | | | |
| Processor Set-up | R0/R1 or R1/R2 | 1 | 1 | | | | 2 |
| | | | | | | | 160 Samples |

These simulations are completed for only positive values of velocity in order to avoid unnecessary data collection. Previous data sets indicate that the performance over the positive and negative Nyquist intervals are symmetrical and provide redundant information. For these runs, one level of SNR (60 dB) is also deleted as this higher value

produces results that are no different than those at 40 dB. The next two figures are the result of the Release 8.04 simulations for the R0/R1 estimator.

Figure 11 is the bias performance data for the R0/R1 estimator for SNR's of 10 to 40 dB. The change in noise management results in improved performance for this estimator over the previous design. However, the estimator still does not meet requirements for SNRs between 10 and 20 dB. For the lower spectrum width values the bias exceeds the required 1 $ms^{-1}$. For SNR's of 20 dB and above however, this version of the estimator is compliant with WSR-88D requirements.

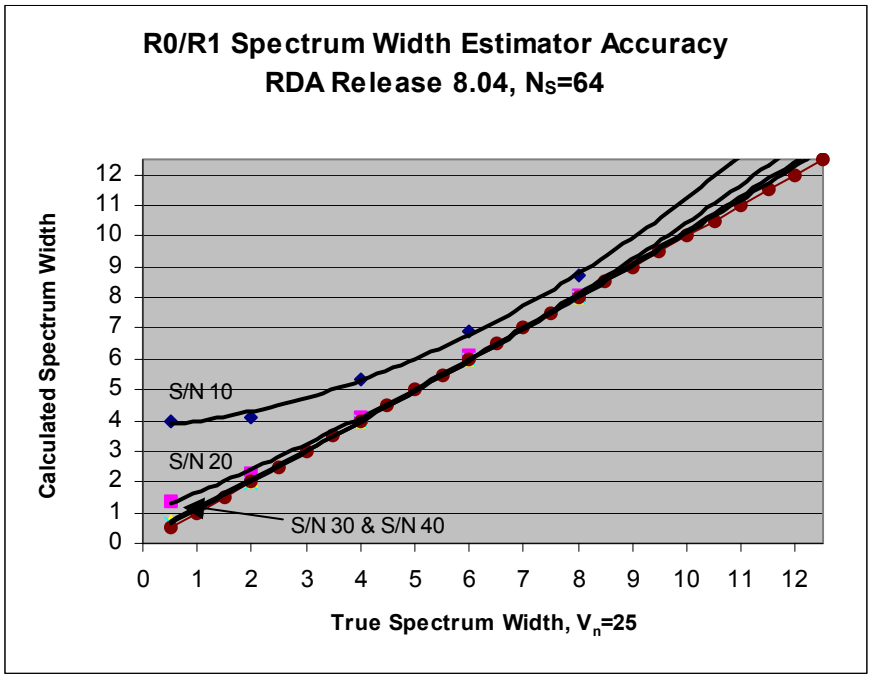


**Figure 11 - R0/R1 Estimator Using System Noise Value**

Figure 12 is the standard deviation of the R0/R1 estimator outputs. The standard deviation performance of this version of the width estimator is also compliant with WSR-88D specifications. In fact, it performs below the required value of 1 $ms^{-1}$ at all but the narrowest widths for SNR = 10 dB.

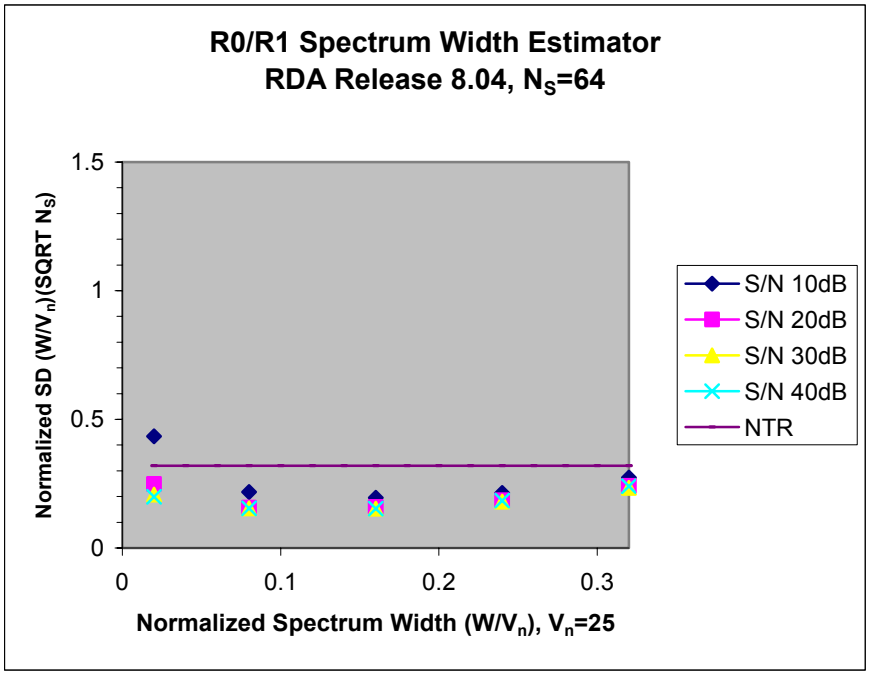


**Figure 12 - Standard Deviation of R0/R1 Using System Noise**

Figure 13 and 14 show the performance of the R1/R2 estimator for Release 8.04, showing the performance of the estimator with system noise as an input rather than as an estimated quantity.

There appears to be a slight improvement in bias performance for this case. The bias is within 1 dB for all values of SNR and true spectrum width. Figure 14 is the standard deviation summary. In comparison to Figure 10, note that the standard deviation has decreased significantly, especially for low values of true spectrum width.

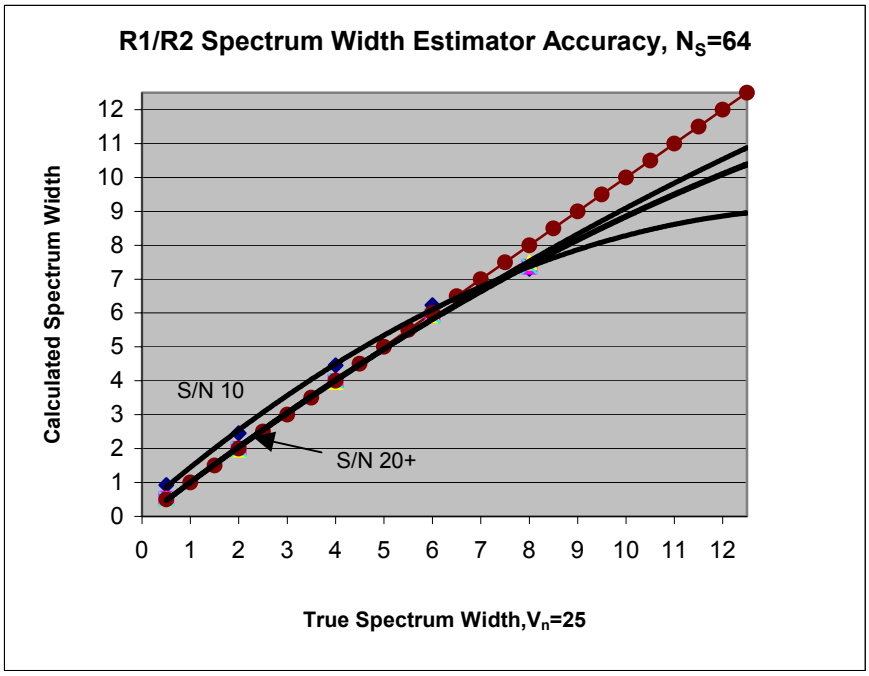


**Figure 13 - R1/R2 Estimator Bias - Using System Noise**

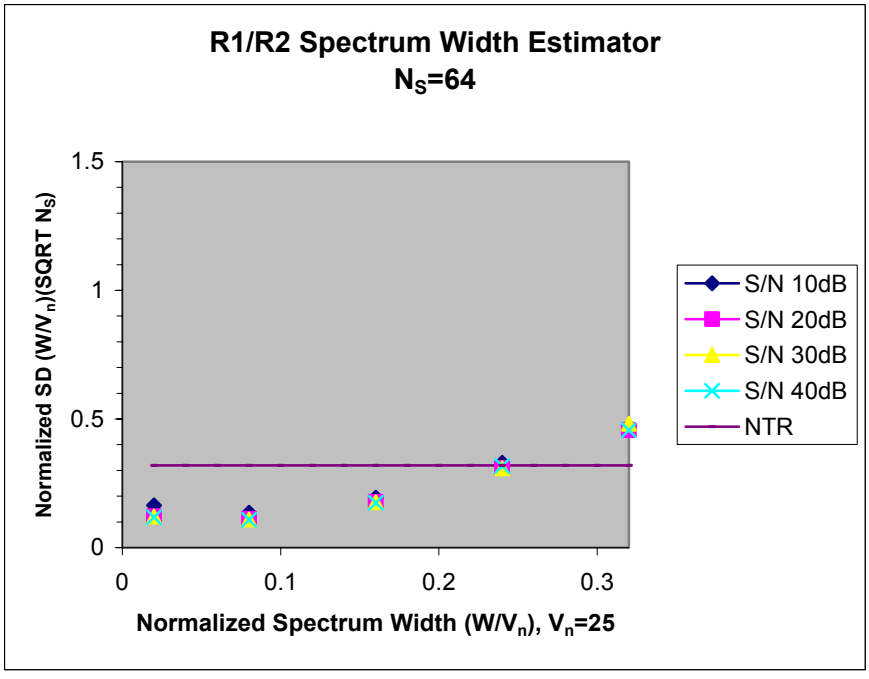


**Figure 14 - Standard Deviation of the R1/R2 Estimator Using System Noise**

One aspect of this simulation is that the system noise level used by the signal processing algorithms is input by the operator. For these simulated cases, the estimators have access to an essentially "perfect" noise measurement. In practice, this noise measurement will come from the system calibration functions and will be subject to possible errors.

Because the R0/R1 bias performance at low signal to noise ratios did not meet requirements, the evaluation team provided these results to SIGMET for further analysis. SIGMET subsequently modified the R0/R1 estimator noise compensation scheme and posted software release 8.04.03. The ROC team became aware of this update on December 3, 2003.

## 6. Evaluation with Noise Compensation for the R0/R1 Estimator (Release 8.04.03)

The ROC engineering team obtained release 8.04.03 and loaded it on the RVP8 systems. The associated Release Notes dated November 18th contain the following relevant text:

"Two improvements have been made to the RVP8 spectrum width estimator:

- The R0/R1 estimator is now corrected for system noise. This removes the bias that used to be present for low SNR cases.

- A correction is now applied to repair the spectral broadening that results when the original time series have been windowed. This is only a concern for narrow spectra having normalized widths less than 0.075 (or so)."

The engineering team ran additional simulations using Release 8.04.03, focusing on bias and standard deviation plots for the two estimators. Signal to noise ratios less than 10 dB were included for the R0/R1 estimator data. New performance data for the spectrum width estimators of release 8.04.03 is depicted in the following four figures (Figures 15 through 18). The data indicates that both estimators are compliant with WSR-88D specifications for Release 8.04.03. Note that the WSR-88D specification is for signals 10 dB and above. For this set of simulations, the team obtained data for signals of 0 and 5 dB SNR as well. Even at these lower levels, the R0/R1 estimator performed well with bias in compliance over a significant portion of the input spectrum width range. However, the standard deviation is above 1 $ms^{-1}$ for all of the 0 dB curve and about half of the 5 dB curve.

The R1/R2 estimator bias for this version is fully compliant for all SNR's equal to or greater than 10 dB and the standard deviation is below 1 $ms^{-1}$ at these SNR's for true widths up to about 7 $ms^{-1}$.

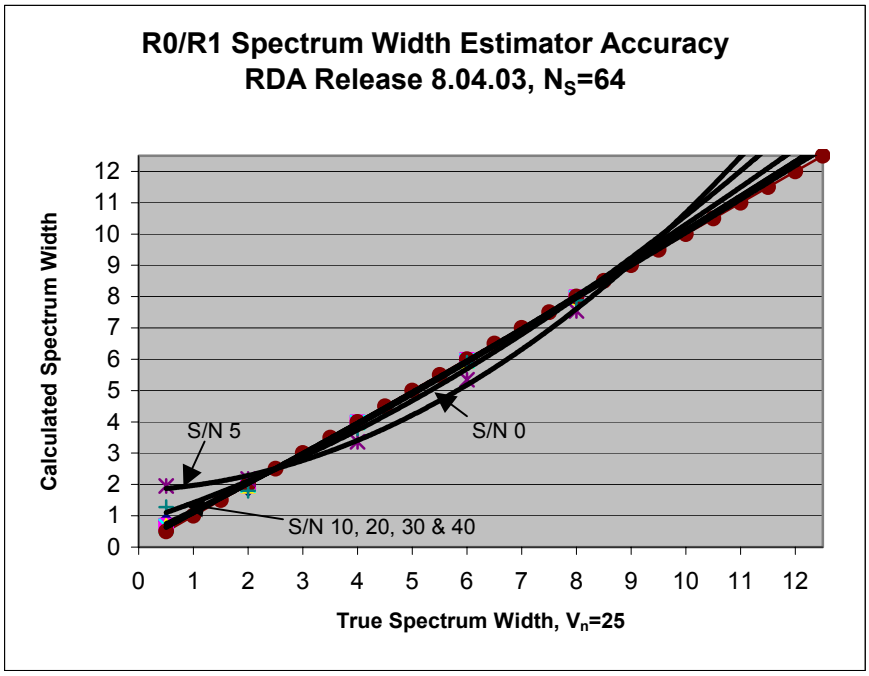


**Figure 15 - R0/R1 Bias - Noise Compensated**

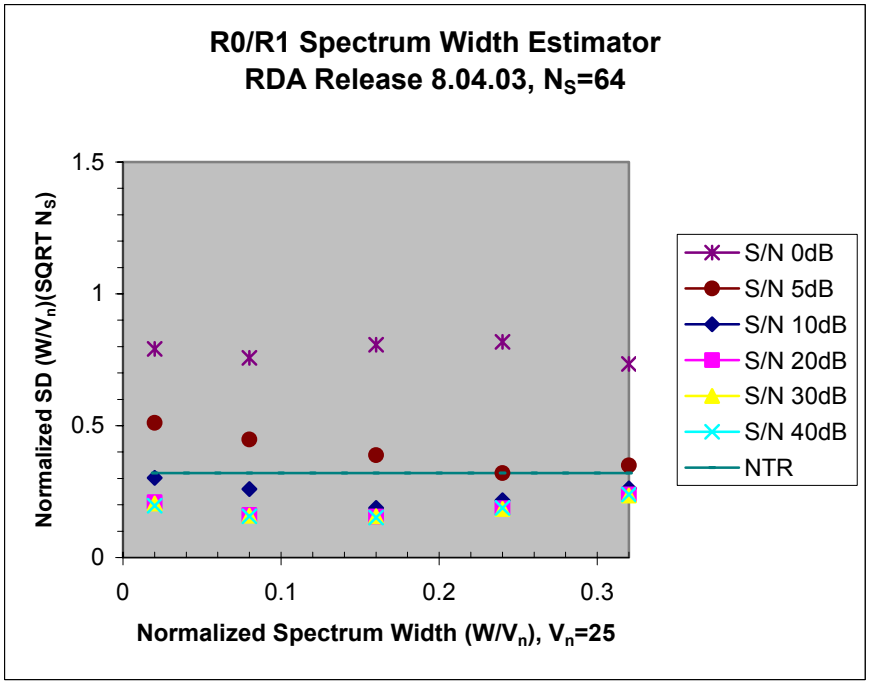


**Figure 16 - R0/R1 Standard Deviation - Noise Compensated**

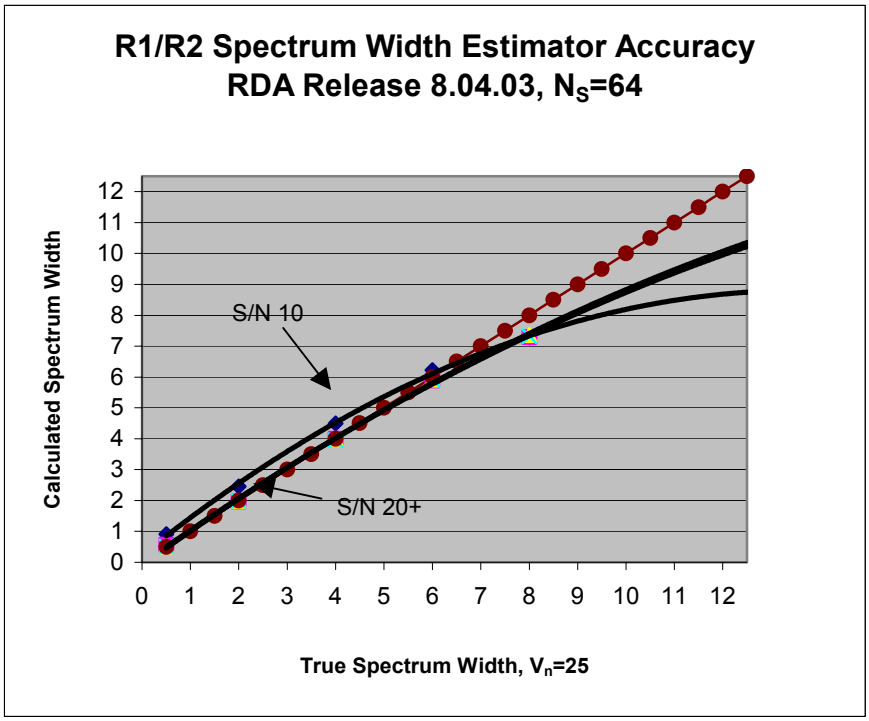


**Figure 17 - R1/R2 Bias - Noise Compensated**

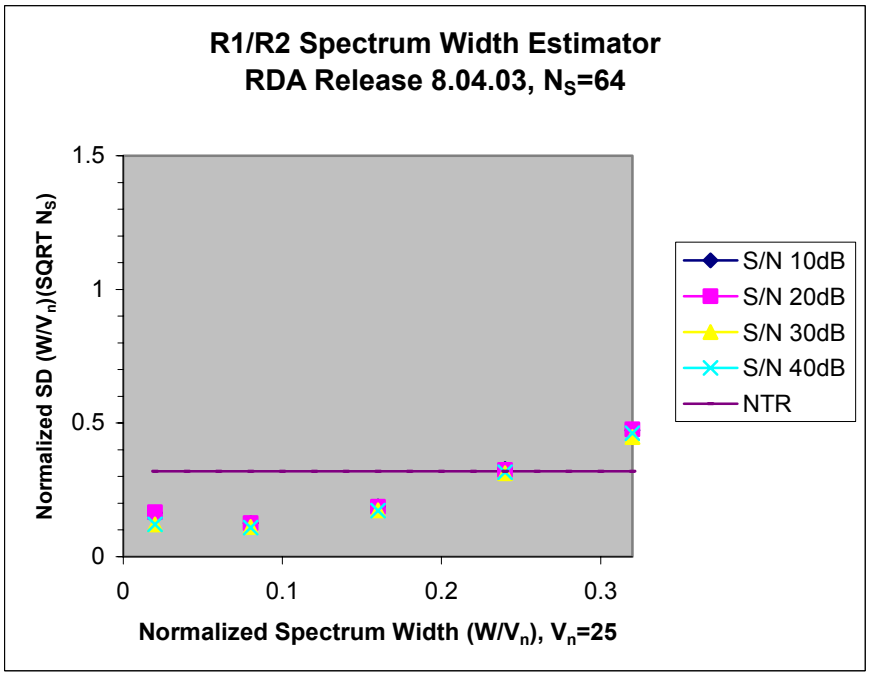


**Figure 18 - R1/R2 Standard Deviation - Noise Compensated**

The R1/R2 estimator exhibits a number of samples bias as expected by theory [6]. Figure 19 is an example of this for the case where PRF = 1000 Hz, SNR = 30 dB and the noise level is at –80 dBm. It can be seen that for widths below 2 $ms^{-1}$ and above 6 $ms^{-1}$, a bias exists for 32 and 64 samples. For sample sizes of 128 and 256, there is essentially no bias.

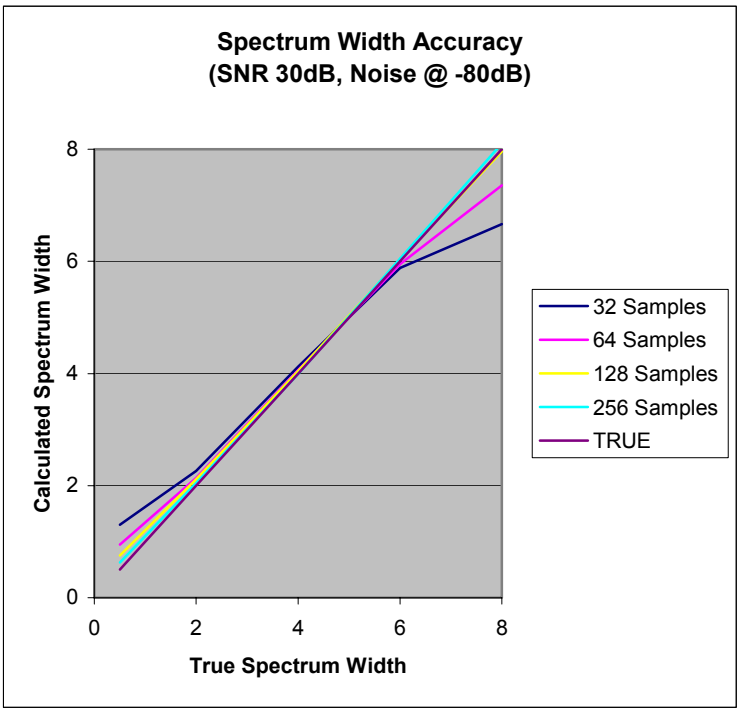


**Figure 19 - Number of Samples Bias for the R1/R2 Estimator**

## 7. ORDA Clutter Suppression and Reflectivity Bias Removal Requirements

In evaluating the GMAP performance two sets of requirements are used. The prime requirements are the high level clutter suppression specifications given the NEXRAD Technical Requirements (NTR) [2]. A secondary guideline is the performance specification for the post filter reflectivity bias correction algorithm under development by the ROC and the National Center for Atmospheric Research.

Ground clutter suppression was originally addressed in section 3.7.1.7 of the NTR. These are now documented in section 3.7.2.7 of the System Specification (SS). Some of the requirements are general and applicable to any suppression method while others are applicable only to a notch filter. The NTR and SS also define the clutter model and parameters to be used for testing against these requirements. The model applicable to this testing is clutter model A which is defined as a Gaussian spectrum centered at zero frequency. The clutter spectrum width (standard deviation) is 0.1 $ms^{-1}$ plus the spectrum width resulting from the antenna rotation rate at the lowest two elevation angles. This imposes requirements in a clutter model having a Gaussian spectrum with zero mean and a standard deviation of 0.32 $ms^{-1}$ at the WSR-88D median wavelength. (Much testing was done at the WSR-88D test spectrum width of 0.28 $ms^{-1}$ to retain continuity with earlier testing).

Ground clutter suppression requirements are established in section 3.7.1.7.1 of the NTR (SS section 3.7.2.7.1). General requirements applicable to any suppression method are:

- A clutter suppression capability of at least 30 dB in the reflectivity channel.
- A clutter suppression selectable between 20 dB and 50 dB in the Doppler channel.
- In areas where the clutter suppression is <u>not</u> applied, there shall be no degradation in the weather return parameter measurement accuracy with respect to the NTR or SS requirements (SD[V] $\leq$ 1 $ms^{-1}$, SD[W] $\leq$ 1 $ms^{-1}$ and SD[Z] $\leq$ 1 dB).

Meteorological signal estimate errors due to the clutter suppression are addressed in section 3.7.1.7.2 of the NTR (SS section 3.7.2.7.2). General requirements are:

- Bias and standard deviation contributions by the clutter suppression device to the mean radial velocity and spectrum width estimates shall be less than 2 $ms^{-1}$.

- The test conditions given in the NTR and SS are specific for a notch filter. General case test conditions are SNR > 20 dB, SCR > 30 dB i.e. high signal with low clutter conditions.

The NTR and SS specifications for reflectivity bias are specific for a notch and not applicable to the GMAP method since GMAP reconstructs the spectra and removes the bias associated with clutter suppression. What is applicable in this case is the specification for the post filter reflectivity bias correction algorithm which has a goal of correction uncertainty of less than 2 dB.

## 8. Overview of GMAP Technique

SIGMET developed the Gaussian Model Adaptive Process (or GMAP) algorithm as an alternative to the originally supplied time domain 4-pole elliptic Infinite Impulse Response (IIR) and frequency domain clutter filters. A joint team of ROC and ORDA engineers evaluated these filters and deemed them unsuitable for the WSR-88D. SIGMET developed GMAP in response. GMAP offers considerable advantage over both the original SIGMET 4-pole and WSR-88D legacy 5-pole IIR filters. IIR filters exhibit a number of undesirable characteristics including high reflectivity bias for signals near the zero isotach and azimuthal smearing. IIR filters also require initialization and reconfiguring for each PRF and also introduce signal phase distortion which make them unsuitable for use with the phase coding algorithms planned for ORDA [11].

GMAP first uses a Discrete Fourier Transform (DFT) converting the input time series to the frequency domain. Signal, noise, and clutter removal along with signal restoration is all performed in the frequency domain. The resultant spectrum is then converted back to the time domain via an Inverse DFT for input to the estimators.

SIGMET provided the following description of GMAP [7]:

"The GMAP clutter filter incorporates signal modeling, clutter modeling, and rank order spectral analysis to provide a robust filter that can operate over a wide range of conditions. GMAP works from an input spectrum containing unknown amounts of clutter, signal, and noise, and returns an output spectrum with the clutter influence removed. The algorithm requires only a single tuning parameter 'Wc' (the assumed clutter width in $ms^{-1}$), and can be summarized as follows:

- Convert the input spectral values to dB and sort the entire collection of points in order of increasing power. This gives us a rank ordered power spectrum, along with indices of each point in the original DFT.

- Analyze the noise and signal characteristics of the rank ordered spectrum to deduce the noise power and spectral signal point, i.e., the point beyond which we seem to have signal statistics rather than noise statistics. Note that this uses the same set of procedures as the whitening algorithm for Random Phase mode. (The algorithm can also accept the time domain system noise measurement.)

- Create a model for windowed Gaussian clutter having a normalized spectrum width based on the input value 'Wc' and the current wavelength and PRF. The clutter model also takes account of the particular window and spectrum size being used.

- Calculate the power ratio between the mean of the middle three points of the clutter model and the middle three points of the original spectrum. Search the clutter model outward from DC for the point at which it drops below the noise level from #2. This tells us the width that clutter of this power would occupy within this spectrum, and defines the 'clutter gap' of points to be removed around zero velocity.

- If we found a trusted signal cut in #2 from the rank ordered spectrum, then fit a Gaussian model to the spectral points that seem to represent valid weather signal. First calculate R0&R1 from the sparse spectrum containing only those 'intelligent' points, minus whichever ones are being discarded from the clutter gap.

- Proceed with modeling and interpolating the clutter gap region of the spectrum. The procedure is an iterative one, in which we fill the gap with modeled points, and then recompute the model parameters based on the R0&R1 from #5, combined with these new trial points. Continue until no significant signal power is added back into the clutter gap, at which point we assume that we've reconstructed whatever original signal power was lost in the clutter gap."

As described above, GMAP operates in the frequency domain, analyzing spectral components associated with the clutter and weather signals as well as system noise levels. The end result is a spectrum which has the clutter components removed and replaced with expected signal components, generated using a Gaussian model. Figure 20 is a good example of the spectral output of this signal restoration process.

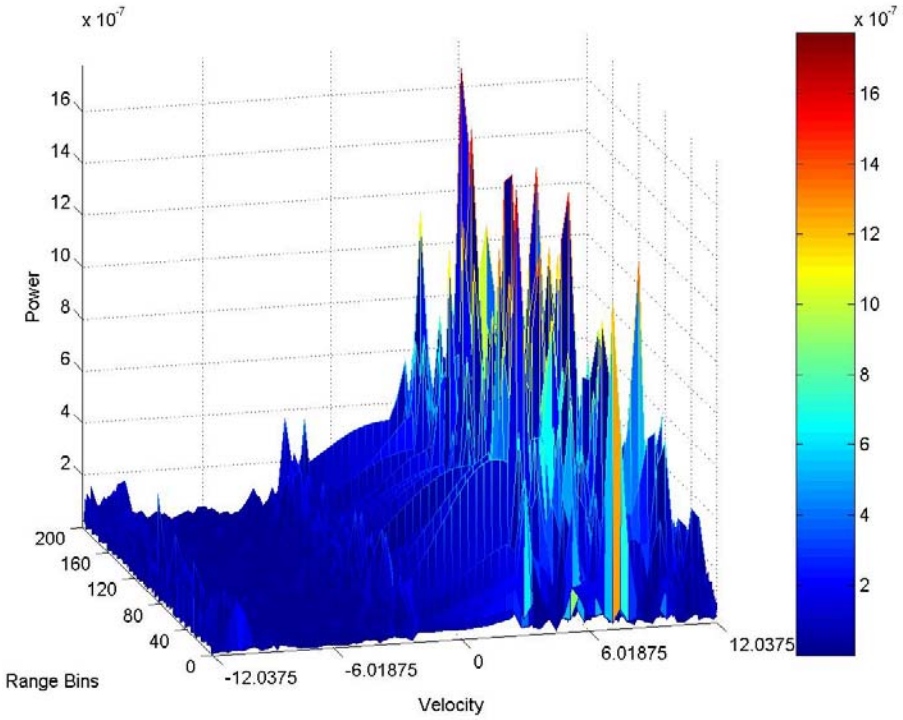


**Figure 20 - Spectra Resulting from GMAP Processing**

In this figure, 200 spectral plots are displayed. This is a sample taken from the clear air mode studies, with a PRF of 450 Hz. The signal to noise ratio is only 10 dB while the clutter to signal ratio is 50 dB. The simulated weather signal is located between 0 and the upper Nyquist bound (in this case about 12 $ms^{-1}$). The center velocity of the simulated signal is 4.8 $ms^{-1}$ and the spectrum width is 4 $ms^{-1}$. In this case a small portion of the signal spectrum can be seen folded around to the negative Nyquist interval (the components around –12). The area of interest however is that portion of the spectrum centered around 0 velocity. This is the area where the clutter signal has been suppressed and replaced with computed weather signal components. The area where clutter components have been suppressed and replaced with Gaussian model spectral

coefficients can be seen clearly in this example. The GMAP process then performs an inverse DFT on these spectra to produce time series inputs for the estimators.

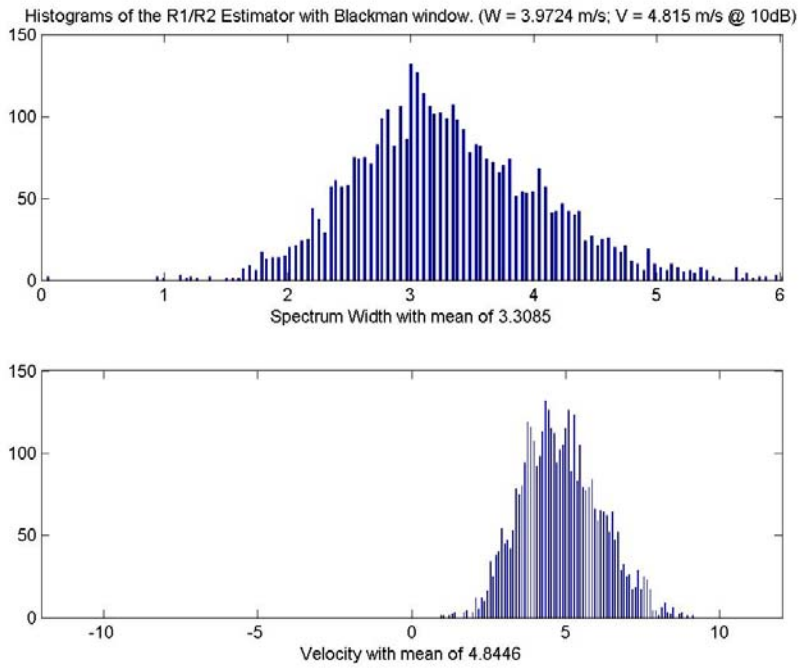


**Figure 21 - Histogram from Clear Air Example of Fig 20**

Figure 21 is the histogram associated with the case in Figure 20. This depicts a statistical summary of the estimator outputs for velocity and spectrum width. The estimators operated on the time series data resulting from the Inverse DFT of the GMAP process after the clutter is removed and the signal coefficients restored. As can be seen, the estimators are able to correctly determine the mean values of velocity and spectrum width from the reconstructed spectra. In this case the velocity estimate is quite good with the mean of the output data points at 4.8446 $ms^{-1}$ versus the input simulated mean of 4.815 $ms^{-1}$.

The performance of GMAP, i.e. the clutter suppression achieved and the variances of the Doppler moments retrieved, is sensitive to a number of factors. The more important ones appear to be the assumed clutter width, the window function, and the number of samples. During the initial simulations, it became evident that the process did not meet requirements for the case of N = 16 data samples, a scenario related to the severe weather surveillance mode. SIGMET subsequently concluded that the rank order noise estimation routine used by GMAP was not working for such low sample inputs and modified the algorithm to use the supplied system noise level instead. This change is incorporated in Release 8.04.

High suppression (50 dB) requires an aggressive window function such as the Hamming or Blackman. Testing included both Hamming and Blackman as well as the GMAP adaptive window selection. Results from the adaptive window process were not significantly better than those with the Blackman window. The data in this report is focused primarily on the performance of GMAP using the Hamming and Blackman windows.

All things being equal there is an increase in moment standard deviation due to the processing. The amount of increase varies with the moment, but generally is about a factor of 1.6. There is also a number of samples dependency i.e. moment standard deviation varies inversely with the square root of the number of samples.

## 9. Performance of the GMAP Technique

As mentioned the performance of the GMAP algorithm is sensitive to the window function used and the number of samples available. The window function is under processing control but the number of samples is determined by the radar acquisition

mode. The three windows tested were the Rectangular, Hamming, and Blackman. The team also collected data using the adaptive window selection process supported by GMAP. In this mode, GMAP attempts to select the optimal window performance, choosing between Rectangular, Hamming, or Blackman.

Results with the adaptive window selection technique indicate it does not significantly improve performance at this stage of development.

The Rectangular window function delivers acceptable performance only for clutter to signal ratios less than 0 dB and thus has little utility for ORDA clutter filtering.

Based on these two observations, the data collection and analysis efforts focused primarily on the performance of GMAP with selection of the Blackman and Hamming windows.

Figure 22 compares the shapes of the Blackman and Hamming windows in the time domain applicable to a 50 point transform generated by MATLAB functions.

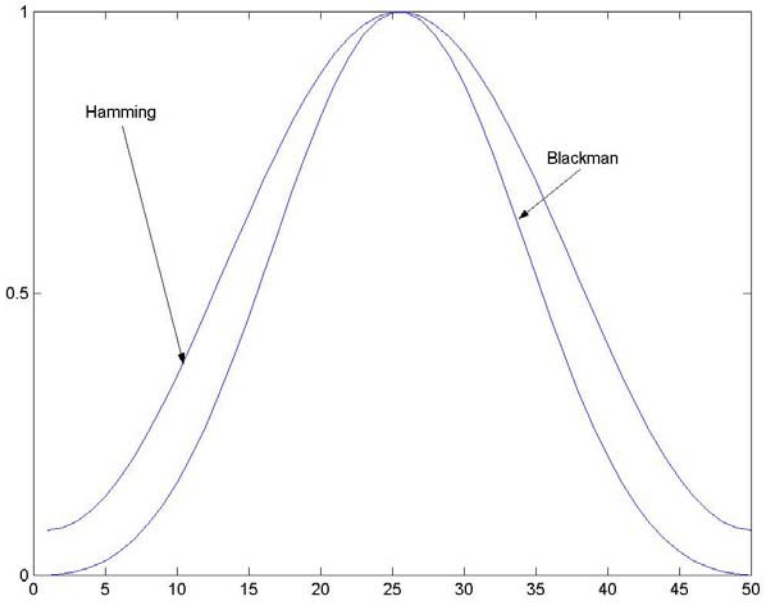


**Figure 22 - Shapes of Blackman and Hamming Window Functions**

These window functions are normalized with a maximum value of 1 at the center of the spectrum. The Blackman window can be seen to be more aggressive in suppressing spectral coefficients at the edges of the window, and thus result in a loss of signal information.

The Hamming window will provide a clutter suppression of 30 dB and the Blackman will provide a clutter suppression of 50 dB. The Hamming provides a slightly smaller standard deviation of estimate than the Blackman window under similar conditions. For a complete discussion of window functions see [3].

An example of GMAP performance in clutter suppression and signal recovery of weak signal in the presence of strong clutter is given in Tables 3 and 4. All measurements were taken using the R1/R2 spectrum width estimator.

Signal parameters are:

Nyquist Velocity, $V_n = 26.8\ ms^{-1}$
Signal to Noise Ratio, SNR = 10 dB
Signal Spectrum Width, $W_S = 4\ ms^{-1}$
Width Estimator, R1/R2
Clutter Spectrum Width, $W_C = 0.28\ ms^{-1}$
Number of Samples, $N_S = 64$
Pulse Repetition Frequency, PRF = 1000 Hz

Table 3 - GMAP Performance - Blackman - Noise Estimation

| CSR (dB) | $P^*_{bias}$ (dB) | SD[P] (dB) | $V_{bias}$ ($ms^{-1}$) | SD[V] ($ms^{-1}$) | $W_{bias}$ ($ms^{-1}$) | SD[W] ($ms^{-1}$) |
|---|---|---|---|---|---|---|
| 50 | 0.04 | 2.01 | 0.88 | 1.26 | -0.16 | 1.50 |
| 40 | -0.22 | 1.80 | 1.07 | 1.26 | -0.08 | 0.91 |
| 30 | 0.17 | 1.92 | 0.54 | 1.29 | -0.16 | 0.86 |
| 20 | 0.17 | 1.91 | 0.59 | 1.21 | -0.13 | 0.88 |
| 10 | 0.18 | 1.79 | 0.27 | 1.21 | -0.08 | 0.86 |
| 0 | -0.015 | 1.59 | 0.35 | 1.21 | -0.11 | 0.86 |
| none | -0.16 | 1.45 | 0.54 | 1.18 | -0.05 | 0.88 |

These entries are the average over the Nyquist interval
* $E_{ST}$ = True + Bias

Table 4 - GMAP Performance - Hamming – Noise Estimation

| CSR (dB) | $P_{bias}$ (dB) | SD[P] (dB) | $V_{bias}$ ($ms^{-1}$) | SD[V] ($ms^{-1}$) | $W_{bias}$ ($ms^{-1}$) | SD[W] ($ms^{-1}$) |
|---|---|---|---|---|---|---|
| 30 | 0.18 | 1.91 | 1.10 | 1.96 | -0.32 | 1.23 |
| 20 | 0.18 | 1.64 | 0.54 | 1.13 | -0.13 | 0.78 |
| 10 | 0.15 | 1.57 | 0.19 | 1.10 | -0.11 | 0.78 |
| 0 | -0.05 | 1.43 | 0.16 | 1.07 | -0.08 | 0.75 |
| none | 0.10 | 1.29 | 0.16 | 1.05 | -0.05 | 0.75 |

These entries are the average over the Nyquist interval

As seen from Tables 3 and 4 the GMAP algorithm using the Blackman window can recover signals in the presence of clutter with acceptable bias and standard deviation for clutter to signal ratios less than 50 dB, which in this case is a clutter to noise suppression of 60 dB. Using the Hamming window the recovery range is 30 dB (clutter to noise of 40 dB), but the recovered signal has lower bias and standard deviation (about 10 % lower). This can be taken advantage of in the Adaptive mode of GMAP which selects the least aggressive window needed for satisfactory signal recovery.

There is an increase in standard deviation of the spectral moment estimates due to the GMAP technique. Standard deviation of the power estimate at SNR > 10 dB with no range averaging is [3]:

$$SD[P] = 10 \log\left[1 + \frac{1}{\left(4\frac{\sqrt{\pi}\ N\ T_S\ W}{\lambda}\right)^{1/2}}\right]$$

Which for the parameters of Table 3 and 4 is:

$$SD[P] = 0.92 \text{ dB}$$

By inspection it is seen that for no clutter the standard deviation of the signal power estimate with the Blackman window is 1.45 dB (a ratio of 1.57 times the theoretical value) and 1.29 dB with the Hamming. At a clutter to signal ratio of 30 dB the standard deviation is 1.92 dB with the Blackman and 1.91 dB with the Hamming.

The 1 km reflectivity estimate is an average of four 250 meter range cells and has standard deviation one half the above values i.e. the standard deviation ranges from 0.7 dB for the Hamming window and weak clutter to 1.0 dB for the Blackman window and a CSR of 50 dB. This has some implication for the planned incorporation of high resolution products. For 250 km reflectivity products, the standard deviation can be somewhat greater than 2 dB, which is the preferred limit. However, this same issue occurs with the legacy performance and is being addressed in the research community with techniques such as over sampling in range with the potential for variance reduction through the use of a whitening technique[12].

Standard deviation of the velocity estimate is given by [5]

$$SD[V] = \frac{\lambda}{2}\left(\frac{w}{4\sqrt{\pi}\,\beta^2(T_S)NT_S}\right)^{1/2}$$

where w is the frequency spectrum width and $\beta$ is the correlation between samples. For the assumed Gaussian spectrum, $\beta = \exp(-2\pi^2 w^2 T_S^2)$.

For the parameters of Tables 3 and 4

$$SD[V] = 0.75\ ms^{-1}$$

From Table 3 it is seen that the Blackman window delivers a velocity estimate standard deviation ranging from 1.18 $ms^{-1}$ for no clutter (again, a ratio of 1.57 times the theoretical

value) to 2.06 $ms^{-1}$ for a CSR of 50 dB. The Hamming delivers a standard deviation of 1.05 $ms^{-1}$ with no clutter to 1.96 $ms^{-1}$ at a CSR of 30 dB. At a CSR of 30 dB the Blackman delivers a standard deviation of 1.26 $ms^{-1}$.

For the parameters given in Tables 3 and 4 the standard deviation of the R1/R2 width estimator is 0.67$ms^{-1}$ [6]. The Blackman window delivers a width estimate having standard deviation of 0.88 $ms^{-1}$ with no clutter (ratio to theory of 1.51) to 1.5 $ms^{-1}$ for CSR of 50 dB with values of 0.86 $ms^{-1}$ at CSR of 30 dB. For the Hamming the standard deviation ranges from 0.75 $ms^{-1}$ with no clutter to 1.23 $ms^{-1}$ for CSR of 30 dB. Spectrum width is the least sensitive to the GMAP estimate variance increase.

As seen from Tables 3 and 4, for the given processing parameters, the residual bias in all three moment estimates is small compared to the standard error of estimate and well within specifications. Velocity and width bias and standard deviation are less than 2 $ms^{-1}$ and reflectivity bias is a few tenths of a dB and standard deviation (1 km) is about 1 dB.

During the initial GMAP simulations, the team noted that algorithm performance for low numbers of samples (N = 16) did not meet specifications. SIGMET subsequently determined that the rank order noise estimation process was unable to reliably separate signal from noise using spectra generated with these low numbers of coefficients. As a result SIGMET provided RVP8 software release 8.04 which uses the supplied system noise value rather than the output of the rank order method. The team completed additional simulations and verified that the GMAP algorithm performed satisfactorily with the change. All the data presented in the remainder of this report is generated using either release 8.04 or a subsequent release (8.04.03).

Other aspects of GMAP behavior are shown in Tables 5 and 6. These tables contain bias and standard deviation data for power, velocity, and spectrum width as a function of clutter to signal ratio. Signal parameters are the same as previously except that both clutter and signal have zero mean velocity and noise is the measured system noise (release 8.04) rather than the estimated value using the rank order technique.

Table 5 - GMAP Performance – Blackman - System Noise Value

| CSR (dB) | $P_{bias}$ (dB) | SD[P] (dB) | $V_{bias}$ ($ms^{-1}$) | SD[V] ($ms^{-1}$) | $W_{bias}$ ($ms^{-1}$) | SD[W] ($ms^{-1}$) |
|---|---|---|---|---|---|---|
| 60 | 3.88 | 3.24 | -0.01 | 0.72 | 0.22 | 0.52 |
| 50 | 0.25 | 2.28 | 0.06 | 1.10 | 0.03 | 0.72 |
| 40 | -0.44 | 2.29 | -0.05 | 1.23 | -0.09 | 0.88 |
| 30 | -0.35 | 2.23 | -0.05 | 1.17 | -0.07 | 0.88 |
| 20 | -0.37 | 2.20 | 0 | 1.16 | 0.02 | 0.83 |
| 10 | -0.36 | 2.16 | 0 | 1.12 | 0.02 | 0.83 |
| 0 | -0.32 | 2.07 | -0.02 | 1.12 | 0.12 | 0.86 |

Note: Entries are the average over the Nyquist interval

Table 6 - GMAP Performance – Hamming - System Noise Value

| CSR (dB) | $P_{bias}$ (dB) | SD[P] (dB) | $V_{bias}$ ($ms^{-1}$) | SD[V] ($ms^{-1}$) | $W_{bias}$ ($ms^{-1}$) | SD[W] ($ms^{-1}$) |
|---|---|---|---|---|---|---|
| 60 | 23.3 | 5.43 | 0.01 | 0.50 | -2.45 | 0.17 |
| 50 | 13.6 | 5.10 | -0.01 | 0.44 | -2.33 | 0.36 |
| 40 | 5.25 | 3.48 | 0.02 | 0.56 | -1.82 | 0.67 |
| 30 | 0.45 | 1.83 | -0.03 | 0.93 | -0.92 | 0.85 |
| 20 | -0.31 | 1.89 | -0.005 | 1.00 | -0.19 | 0.78 |
| 10 | -0.22 | 1.84 | 0.004 | 1.00 | 0.03 | 0.76 |
| 0 | -0.25 | 1.74 | 0.04 | 1.00 | 0.02 | 0.76 |

Note: Entries are the average over the Nyquist interval

Plots of the data related to reflectivity bias performance are shown in Figures 23 and 24. These plots show the output SNR as a function of CSR for an input SNR of 10 dB.

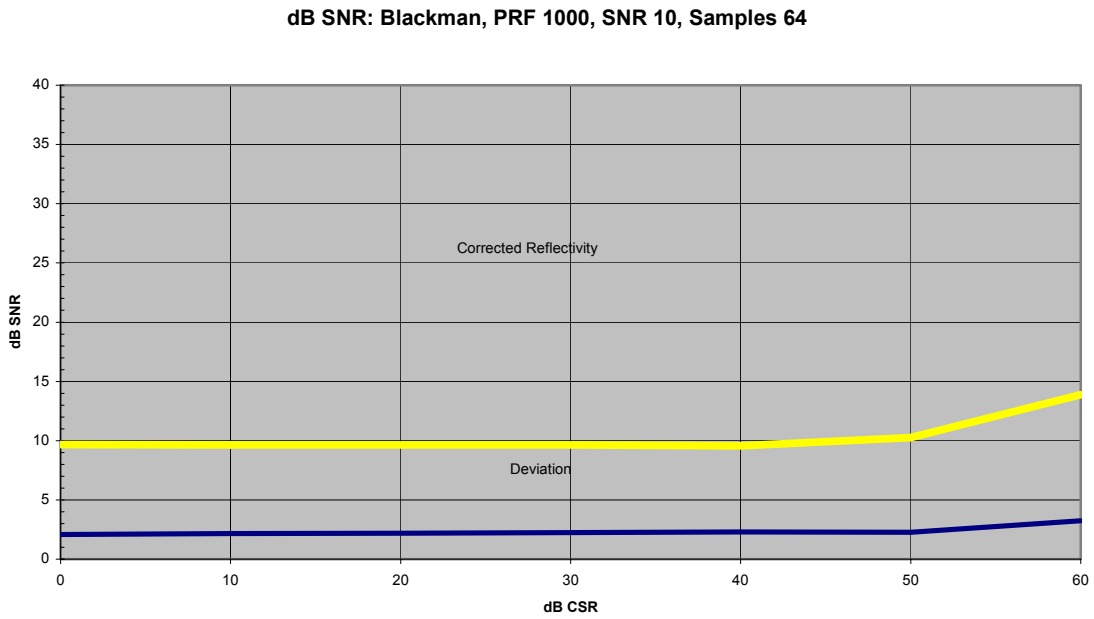


**Figure 23 - Signal Power Bias - Blackman Window**

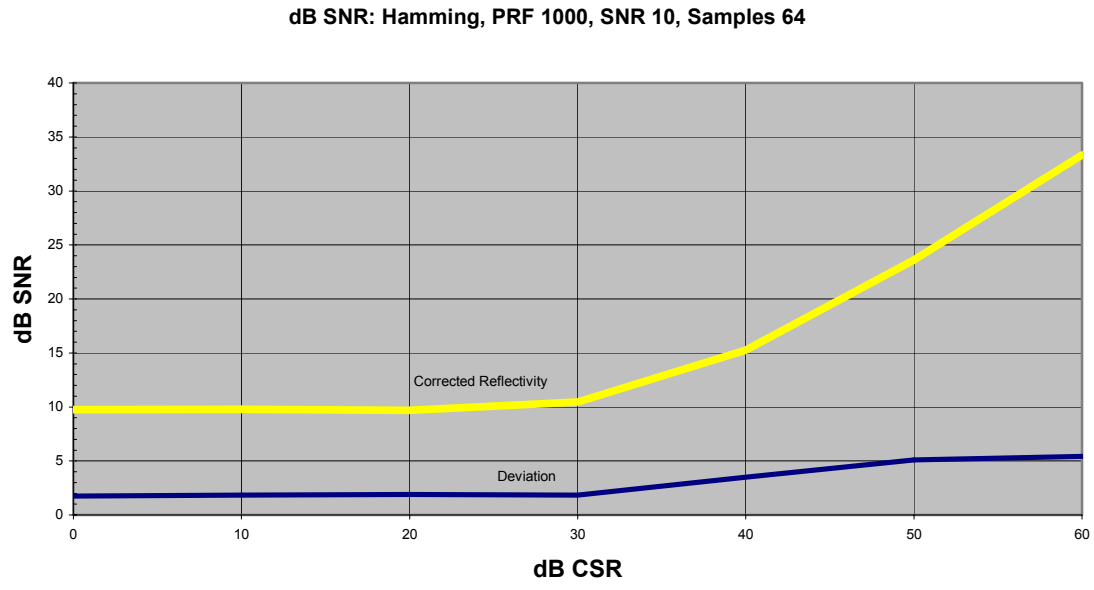


**Figure 24 - Signal Power Bias - Hamming Window**

Note from Table 5 and Figure 23 that the Blackman window delivers specification compliant performance for CSR less than about 55 dB (post bias correction uncertainty of

2 dB). From Table 6 and Figure 24 it is seen that the Hamming window is compliant only for CSR less than about 33 dB but in this region delivers a smaller standard deviation of estimate than the Blackman. Signal recovery is difficult for zero velocity signals with the legacy notch filter [8], however the GMAP handles this situation very well.

## 10. GMAP Performance Related to Convective Surveillance Mode

The WSR-88D has two modes of operation, convective mode and clear air mode. The convective mode uses VCP 11, VCP 21, and the experimental VCP 12. The clear air mode uses VCP 31 and VCP 32. All convective mode VCP's use redundant scans of the lower elevation angles where reflectivity data is taken at a low PRF (~322 Hz) and Doppler data is taken at a high PRF (>1000 Hz).

Convective mode surveillance data (reflectivity) consists of a small number of samples ranging from 16 with VCP 11 and VCP 12 to 28 with VCP 21. Four of the 250 meter range cells are averaged to form the 1 km output and since the 250 meter estimates are essentially independent, the standard deviation of the 1 km output is one half that of the 250 meter estimate.

Worst case surveillance power estimates are given in Table 7 and 8. This is the minimum number of samples and in practice the DFT will use all available samples resulting in a lower standard deviation of estimate. Signal parameters for Tables 7 and 8 are given here;

Nyquist Velocity = 8.6 $ms^{-1}$
Signal Spectrum width = 4 $ms^{-1}$
Clutter Spectrum Width = 0.28 $ms^{-1}$
Number of Samples = 16
Pulse Repetition Frequency = 322 Hz

From examination of Tables 7 and 8 one may reach the following conclusions:

The bias for the surveillance power estimates are specification compliant (< 2 dB) and ranges from an underestimate of about 1.3 dB to an overestimate of about 0.7 dB.

The standard deviation of the 250 m surveillance power estimate is also specification compliant (< 4 dB) and ranges from about 2 dB to 3 dB. Standard deviation of the 1 km reflectivity estimate will be about 1 dB to 1.5 dB under the benchmark conditions tested.

Table 7 - Surveillance Data – Reflectivity; N = 16, SNR = 10 dB
GMAP Performance - Blackman Window - System Noise as an Input

| | CSR= 10 dB | | CSR = 30 dB | | CSR = 50 dB | |
|---|---|---|---|---|---|---|
| $V/V_n$ | $P_{bias}$ (dB) | SD[P] (dB) | $P_{bias}$ (dB) | SD[P] (dB) | $P_{bias}$ (dB) | SD[P] (dB) |
| 0.0 | -0.91 | 2.85 | -1.13 | 3.29 | 0.60 | 3.14 |
| 0.1 | -0.99 | 2.91 | -1.06 | 3.36 | -0.43 | 3.18 |
| 0.2 | -0.88 | 2.82 | -1.24 | 3.37 | -0.43 | 3.21 |
| 0.3 | -0.90 | 2.84 | -1.01 | 3.11 | -0.24 | 3.04 |
| 0.4 | -0.95 | 2.71 | -0.89 | 2.94 | -0.16 | 3.05 |
| 0.5 | -0.70 | 2.64 | -0.8 | 2.78 | -0.17 | 2.95 |
| 0.6 | -0.65 | 2.51 | -0.56 | 2.75 | 0.21 | 2.90 |
| 0.7 | -0.46 | 2.46 | -0.46 | 2.5 | 0.45 | 2.87 |
| 0.8 | -0.41 | 2.42 | -0.31 | 2.45 | 0.59 | 2.76 |
| 0.9 | -0.25 | 2.27 | -0.25 | 2.31 | 0.68 | 2.76 |
| 1.0 | -0.25 | 2.31 | -0.24 | 2.34 | 0.64 | 2.65 |
| Averages | -0.67 | 2.54 dB | -0.72 | 2.84 dB | 0.16 | 2.96 dB |
| Avg 1 km | | 1.27 dB | | 1.42 dB | | 1.48 dB |

Table 8 - Surveillance Data – Reflectivity - $N_S$ = 16, SNR = 30 dB
GMAP Performance - Blackman Window - System Noise as an Input

| | CSR= 10 dB | | CSR = 30 dB | | CSR = 50 dB | |
|---|---|---|---|---|---|---|
| $V/V_n$ | $P_{bias}$ (dB) | SD[P] (dB) | $P_{bias}$ (dB) | SD[P] (dB) | $P_{bias}$ (dB) | SD[P] (dB) |
| 0.0 | -0.82 | 2.57 | -1.26 | 3.03 | -0.52 | 2.96 |
| 0.1 | -0.94 | 2.61 | -1.18 | 2.92 | -0.43 | 2.93 |
| 0.2 | -0.76 | 2.54 | -1.17 | 2.86 | -0.44 | 2.88 |
| 0.3 | -0.79 | 2.41 | -1.09 | 2.91 | -0.34 | 2.86 |
| 0.4 | -0.75 | 2.53 | -0.92 | 2.79 | -0.07 | 2.88 |
| 0.5 | -0.65 | 2.68 | -0.74 | 2.62 | 0.04 | 2.75 |
| 0.6 | -0.60 | 2.41 | -0.52 | 2.56 | 0.32 | 2.66 |
| 0.7 | -0.39 | 2.14 | -0.39 | 2.41 | 0.40 | 2.66 |
| 0.8 | -0.31 | 2.16 | -0.27 | 2.29 | 0.60 | 2.55 |
| 0.9 | -0.23 | 2.11 | -0.19 | 2.12 | 0.60 | 2.57 |
| 1.0 | -0.23 | 2.09 | -0.16 | 2.19 | 0.67 | 2.60 |
| Averages | -0.59 | 2.39 dB | -0.72 | 2.61 dB | 0.08 | 2.75 dB |
| Avg 1 km | | 1.18 dB | | 1.31 dB | | 1.37 dB |

Convective mode Doppler data is acquired with a high PRF and with number of samples ranging from about 32 using PRF 5 in VCP 12 to 111 using PRF 8 in VCP 21. With PRF 5 the lowest of the legacy PRF's and thus the worst case, the minimum number of samples is 30 in VCP 12, 41 in VCP 11 and 70 in VCP 21. Sample sizes of 32 and 64 brackets the worst case performance of the Doppler moment estimation. The general performance for 64 samples is shown in Table 3 for spectral noise estimation and Table 5 for system noise as an input parameter. As can be seen the performance is specification compliant under the conditions given.

## 11. GMAP Doppler Mode Performance Analysis

The ROC team collected and analyzed an extensive set of data related to the Doppler mode of operation. For this data collection, the PRF is set to 1000 Hz with the

number of samples set for 32 and 64. This parameter set contains operationally relevant values for the Doppler modes. Tables 9 through 12 summarize the performance data for reflectivity measurements. Tables 13 through 16 cover velocity performance and Tables 17 through 20 summarize width performance data.

In the batch mode and contiguous Doppler scans at higher elevation angles the reflectivity estimate is made from the Doppler waveforms. Performance of the GMAP scheme is given in Tables 9 and 10 for two SNR's and three CSR's and a sample size of 32 with Nyquist velocity of 26.8 $ms^{-1}$. By inspection performance is seen to be compliant under these conditions.

Table 9 - Doppler Data – Reflectivity; $N_S = 32$, SNR = 10 dB
GMAP Performance - Blackman Window - System Noise as an Input

| | CSR= 10 dB | | CSR = 30 dB | | CSR = 50 dB | |
|---|---|---|---|---|---|---|
| $V/V_n$ | $P_{bias}$ (dB) | SD[P] (dB) | $P_{bias}$ (dB) | SD[P] (dB) | $P_{bias}$ (dB) | SD[P] (dB) |
| 0.0 | -1.12 | 3.42 | -1.12 | 3.75 | -1.32 | 3.55 |
| 0.1 | -1.78 | 3.34 | -1.73 | 3.83 | -1.28 | 3.79 |
| 0.2 | -1.74 | 3.07 | -1.62 | 3.16 | -0.33 | 3.32 |
| 0.3 | -0.88 | 2.60 | -0.91 | 2.74 | -0.40 | 2.92 |
| 0.4 | -0.56 | 2.43 | -0.55 | 2.54 | 0.74 | 2.41 |
| 0.5 | -0.55 | 2.30 | -0.51 | 2.32 | 0.54 | 2.13 |
| 0.6 | -0.54 | 2.30 | -0.56 | 2.28 | 0.21 | 2.08 |
| 0.7 | -0.57 | 2.27 | -0.54 | 2.25 | 0.05 | 2.13 |
| 0.8 | -0.60 | 2.31 | -0.56 | 2.26 | -0.05 | 2.07 |
| 0.9 | -0.58 | 2.27 | -0.59 | 2.34 | -0.09 | 2.10 |
| 1.0 | -0.54 | 2.25 | -0.60 | 2.32 | -0.08 | 2.16 |
| Averages | -0.86 | 2.6 | -0.84 | 2.71 | -0.18 | 2.61 |
| Avg 1 km | | 1.3 | | 1.36 | | 1.31 |

Table 10 - Doppler Data – Reflectivity; $N_S$ = 32, SNR = 30 dB
GMAP Performance - Blackman Window - System Noise as an Input

| | CSR= 10 dB | | CSR = 30 dB | | CSR = 50 dB | |
|---|---|---|---|---|---|---|
| $V/V_n$ | $P_{bias}$ (dB) | SD[P] (dB) | $P_{bias}$ (dB) | SD[P] (dB) | $P_{bias}$ (dB) | SD[P] (dB) |
| 0.0 | -1.36 | 2.75 | -2.90 | 2.99 | -1.58 | 2.75 |
| 0.1 | -1.41 | 2.89 | -2.69 | 3.09 | -1.08 | 2.88 |
| 0.2 | -1.45 | 2.79 | -2.48 | 2.88 | -0.06 | 2.87 |
| 0.3 | -0.86 | 2.58 | -1.30 | 2.69 | 0.67 | 2.51 |
| 0.4 | -0.59 | 2.35 | -0.64 | 2.35 | 0.72 | 2.26 |
| 0.5 | -0.48 | 2.18 | -0.50 | 2.19 | 0.50 | 2.18 |
| 0.6 | -0.51 | 2.14 | -0.49 | 2.16 | 0.77 | 1.95 |
| 0.7 | -0.51 | 2.26 | -0.56 | 2.22 | 0.04 | 1.90 |
| 0.8 | -0.51 | 2.22 | -0.58 | 2.25 | -0.08 | 2.05 |
| 0.9 | -0.58 | 2.24 | -0.52 | 2.21 | -0.16 | 2.05 |
| 1.0 | -0.57 | 2.17 | -0.48 | 2.27 | -0.10 | 2.06 |
| Averages | -0.8 | 2.42 | -1.19 | 2.48 | -0.03 | 2.31 |
| Avg 1 km | | 1.21 | | 1.24 | | 1.16 |

Some subtle performance characteristics are a larger standard deviation and bias when signal is near clutter (velocity at or near zero), a slight increase in standard deviation at intermediate CSR's (CSR = 30 dB) and of course a decrease in standard deviation with an increase in SNR.

Performance is given in Tables 11 and 12 for the same signal conditions and a sample size of 64. Performance is seen to be compliant with lower standard deviation. The bias is also lower with the larger number of samples implying the GMAP estimate of power has a "number of samples" bias. Note also that in general the bias is skewed negative (underestimate) at low and intermediate CSR's and positive as expected at high CSR and is small compared to the standard deviation.

Table 11 - Doppler Data – Reflectivity; $N_S$ = 64, SNR = 10 dB
GMAP Performance - Blackman Window - System Noise as an Input

| | CSR= 10 dB | | CSR = 30 dB | | CSR = 50 dB | |
|---|---|---|---|---|---|---|
| $V/V_n$ | $P_{bias}$ (dB) | SD[P] (dB) | $P_{bias}$ (dB) | SD[P] (dB) | $P_{bias}$ (dB) | SD[P] (dB) |
| 0.0 | -0.22 | 2.18 | -0.36 | 2.30 | 0.36 | 2.32 |
| 0.1 | -0.44 | 1.91 | -0.67 | 2.24 | 0.09 | 2.39 |
| 0.2 | -0.56 | 1.94 | -0.73 | 1.99 | 0.29 | 2.04 |
| 0.3 | -0.34 | 1.65 | -0.46 | 1.91 | 0.47 | 1.82 |
| 0.4 | -0.28 | 1.63 | -0.28 | 1.72 | 0.49 | 1.60 |
| 0.5 | -0.34 | 1.69 | -0.27 | 1.62 | 0.30 | 1.53 |
| 0.6 | -0.33 | 1.71 | -0.28 | 1.63 | 0.17 | 1.55 |
| 0.7 | -0.28 | 1.68 | -0.29 | 1.68 | 0.13 | 1.56 |
| 0.8 | -0.31 | 1.69 | -0.34 | 1.70 | 0.09 | 1.52 |
| 0.9 | -0.31 | 1.65 | -0.31 | 1.66 | 0.06 | 1.57 |
| 1.0 | -0.32 | 1.72 | -0.31 | 1.67 | 0.04 | 1.57 |
| Averages | -0.34 | 1.77 | -0.39 | 1.83 | 0.23 | 1.77 |
| Avg 1 km | | 0.89 | | 0.92 | | 0.89 |

Overall the standard deviation with 64 samples is less than that with 32 samples by about √2 as expected from statistical theory. At an SNR = 10 dB the standard deviation reduction is about 1.35 for power and 1.54 for velocity. At SNR = 30 dB the reduction factor is about 1.46 for power and 1.45 for velocity. This variation in reduction factor with SNR and signal parameter has implications about the noise introduced by the GMAP processing which has not been analyzed in this report.

Table 12 - Doppler Data – Reflectivity; $N_S$ = 64, SNR = 30 dB
GMAP Performance - Blackman Window - System Noise as an Input

| | CSR= 10 dB | | CSR = 30 dB | | CSR = 50 dB | |
|---|---|---|---|---|---|---|
| $V/V_n$ | $P_{bias}$ (dB) | SD[P] (dB) | $P_{bias}$ (dB) | SD[P] (dB) | $P_{bias}$ (dB) | SD[P] (dB) |
| 0.0 | -0.51 | 2.02 | -0.08 | 2.29 | -0.02 | 2.08 |
| 0.1 | -0.68 | 2.06 | -0.78 | 2.24 | 0.18 | 2.17 |
| 0.2 | -0.60 | 1.91 | -0.87 | 1.96 | 0.33 | 1.99 |
| 0.3 | -0.37 | 1.78 | -0.40 | 1.78 | 0.53 | 1.76 |
| 0.4 | -0.29 | 1.67 | -0.31 | 1.65 | 0.49 | 1.52 |
| 0.5 | -0.27 | 1.63 | -0.26 | 1.55 | 0.32 | 1.46 |
| 0.6 | -0.29 | 1.62 | -0.28 | 1.55 | 0.23 | 1.42 |
| 0.7 | -0.29 | 1.61 | -0.29 | 1.66 | 0.15 | 1.42 |
| 0.8 | -0.32 | 1.63 | -0.28 | 1.58 | 0.06 | 1.59 |
| 0.9 | -0.28 | 1.61 | -0.28 | 1.55 | 0.07 | 1.53 |
| 1.0 | -0.29 | 1.57 | -0.27 | 1.59 | 0.04 | 1.54 |
| Averages | -0.38 | 1.74 | -0.37 | 1.76 | 0.22 | 1.68 |
| Avg 1 km | | 0.87 | | 0.88 | | 0.84 |

Performance of the velocity estimate is given in Tables 13 and 14 for a sample size of 32 and Tables 15 and 16 for 64 samples. By inspection it is seen that performance is compliant to velocity bias less than 2 $ms^{-1}$ but is not fully compliant to a specified velocity standard deviation less than 2 $ms^{-1}$. The standard deviation of velocity exceeds 2 ms-1 at low SNR and high CSR with a sample size of 32. Performance is compliant for a sample size of 64 or larger (see Tables 15 and 16).

The GMAP development is still in the early stages and combinations of custom windows, noise estimation, and other refinements may reduce the standard deviation. In any event, the ability of the scheme to recover the spectral moments on and near the zero isotach, even with large variances, has considerable operational benefit.

.

Table 13 - Doppler Data – Velocity; $N_S$ = 32, SNR = 10 dB
GMAP Performance - Blackman Window - System Noise as an Input

| | CSR= 10 dB | | CSR = 30 dB | | CSR = 50 dB | |
|---|---|---|---|---|---|---|
| $V/V_n$ | $V_{bias}$ ($ms^{-1}$) | SD[V] ($ms^{-1}$) | $V_{bias}$ ($ms^{-1}$) | SD[V] ($ms^{-1}$) | $V_{bias}$ ($ms^{-1}$) | SD[V] ($ms^{-1}$) |
| 0.0 | -0.01 | 2.12 | -0.02 | 2.20 | 0.01 | 2.14 |
| 0.1 | 0.80 | 2.20 | 0.80 | 2.28 | 1.96 | 2.30 |
| 0.2 | 1.18 | 1.98 | 1.05 | 2.04 | -0.43 | 2.30 |
| 0.3 | 0.51 | 2.01 | 0.51 | 2.04 | -1.34 | 2.60 |
| 0.4 | -0.03 | 1.96 | 0.01 | 2.01 | -1.88 | 2.68 |
| 0.5 | -0.07 | 1.88 | -0.16 | 1.93 | -1.93 | 2.95 |
| 0.6 | -0.08 | 1.69 | 0.01 | 1.68 | -1.61 | 2.95 |
| 0.7 | 0.05 | 1.58 | 0.02 | 1.66 | -1.13 | 2.68 |
| 0.8 | 0.02 | 1.77 | 0.01 | 1.77 | -0.86 | 2.95 |
| Averages | 0.26 | 1.91 | 0.25 | 1.96 | -0.8 | 2.62 |

Table 14 - Doppler Data – Velocity; $N_S$ = 32, SNR = 30 dB
GMAP Performance - Blackman Window - System Noise as an Input

| | CSR= 10 dB | | CSR = 30 dB | | CSR = 50 dB | |
|---|---|---|---|---|---|---|
| $V/V_n$ | $V_{bias}$ ($ms^{-1}$) | SD[V] ($ms^{-1}$) | $V_{bias}$ ($ms^{-1}$) | SD[V] ($ms^{-1}$) | $V_{bias}$ ($ms^{-1}$) | SD[V] ($ms^{-1}$) |
| 0.0 | -0.02 | 1.42 | -0.11 | 1.53 | 0.00 | 1.23 |
| 0.1 | 0.39 | 1.47 | 1.07 | 1.61 | -0.15 | 1.34 |
| 0.2 | 0.94 | 1.77 | 1.96 | 1.88 | -0.54 | 1.85 |
| 0.3 | 0.54 | 1.88 | 1.13 | 1.98 | -1.47 | 2.28 |
| 0.4 | 0.05 | 1.88 | 0.16 | 2.09 | -1.85 | 2.68 |
| 0.5 | -0.01 | 1.72 | -0.03 | 1.93 | -1.74 | 2.87 |
| 0.6 | 0.12 | 1.53 | -0.10 | 1.61 | -1.34 | 2.71 |
| 0.7 | 0.11 | 1.42 | 0.11 | 1.47 | -1.07 | 2.65 |
| 0.8 | 0.05 | 1.82 | -0.03 | 1.82 | -0.59 | 2.39 |
| Averages | 0.24 | 1.66 | 0.46 | 1.77 | -0.97 | 2.22 |

Table 15 - Doppler Data – Velocity; $N_S$ = 64, SNR = 10 dB
GMAP Performance - Blackman Window - System Noise as an Input

| | CSR= 10 dB | | CSR = 30 dB | | CSR = 50 dB | |
|---|---|---|---|---|---|---|
| $V/V_n$ | $V_{bias}$ ($ms^{-1}$) | SD[V] ($ms^{-1}$) | $V_{bias}$ ($ms^{-1}$) | SD[V] ($ms^{-1}$) | $V_{bias}$ ($ms^{-1}$) | SD[V] ($ms^{-1}$) |
| 0.0 | -0.01 | 1.13 | 0.05 | 1.13 | 0.04 | 1.02 |
| 0.1 | 0.12 | 1.26 | -0.24 | 1.31 | 0.13 | 1.21 |
| 0.2 | 0.21 | 1.37 | -0.62 | 1.47 | 0.45 | 1.61 |
| 0.3 | 0.15 | 1.31 | -0.32 | 1.47 | 1.02 | 1.88 |
| 0.4 | 0.04 | 1.23 | -0.04 | 1.37 | 1.29 | 2.01 |
| 0.5 | 0.15 | 1.18 | 0.00 | 1.18 | 1.34 | 1.93 |
| 0.6 | 0.07 | 1.17 | -0.02 | 1.19 | 1.05 | 1.90 |
| 0.7 | 0.06 | 1.21 | -0.12 | 1.13 | 0.72 | 1.77 |
| 0.8 | 0.00 | 1.14 | -0.17 | 1.18 | 0.47 | 1.61 |
| Averages | 0.09 | 1.22 | -0.16 | 1.27 | 0.72 | 1.66 |

Table 16 - Doppler Data – Velocity; $N_S$ = 64, SNR = 30 dB
GMAP Performance - Blackman Window - System Noise as an Input

| | CSR= 10 dB | | CSR = 30 dB | | CSR = 50 dB | |
|---|---|---|---|---|---|---|
| $V/V_n$ | $V_{bias}$ ($ms^{-1}$) | SD[V] ($ms^{-1}$) | $V_{bias}$ ($ms^{-1}$) | SD[V] ($ms^{-1}$) | $V_{bias}$ ($ms^{-1}$) | SD[V] ($ms^{-1}$) |
| 0.0 | 0.03 | 1.05 | -0.05 | 1.02 | 0.06 | 0.88 |
| 0.1 | 0.27 | 1.07 | 0.32 | 1.07 | -0.24 | 0.96 |
| 0.2 | 0.32 | 1.28 | 0.62 | 1.42 | -0.54 | 1.39 |
| 0.3 | 0.21 | 1.42 | 0.19 | 1.45 | -1.10 | 1.74 |
| 0.4 | 0.02 | 1.31 | -0.01 | 1.35 | -1.34 | 1.85 |
| 0.5 | 0.04 | 1.15 | -0.08 | 1.15 | -1.23 | 1.80 |
| 0.6 | 0.08 | 1.10 | 0.05 | 1.07 | -0.83 | 1.77 |
| 0.7 | 0.11 | 1.06 | 0.04 | 1.06 | -0.80 | 1.77 |
| 0.8 | 0.05 | 1.06 | 0.10 | 1.07 | -0.46 | 1.61 |
| Averages | 0.13 | 1.17 | 0.13 | 1.18 | -0.72 | 1.53 |

The subtle behavior of the GMAP velocity estimate is different from the power estimate behavior. There is a decrease in standard deviation with an increase in SNR as expected. There is not a pronounced increase in standard deviation when the signal velocity is near the clutter. Generally, the standard deviation maximizes near one half the Nyquist interval, and there is a systematic increase in standard deviation with CSR.

Performance of the GMAP R1/R2 spectrum width estimate is given in Tables 17 and 18 for 32 samples and Tables 19 and 20 for 64 samples.

Table 17 - Doppler Data – Width (R1/R2); $N_S = 32$, SNR = 10 dB
GMAP Performance - Blackman Window - System Noise as an Input

| | CSR= 10 dB | | CSR = 30 dB | | CSR = 50 dB | |
|---|---|---|---|---|---|---|
| $V/V_n$ | $W_{bias}$ ($ms^{-1}$) | SD[W] ($ms^{-1}$) | $W_{bias}$ ($ms^{-1}$) | SD[W] ($ms^{-1}$) | $W_{bias}$ ($ms^{-1}$) | SD[W] ($ms^{-1}$) |
| 0.0 | 0.04 | 1.21 | 0.05 | 1.23 | 0.78 | 1.23 |
| 0.1 | -0.02 | 1.29 | 0.03 | 1.34 | -0.61 | 1.42 |
| 0.2 | -0.40 | 1.23 | -0.38 | 1.26 | -0.59 | 1.52 |
| 0.3 | -0.32 | 1.10 | -0.32 | 1.10 | -0.78 | 1.61 |
| 0.4 | -0.05 | 1.21 | -0.08 | 1.23 | -1.07 | 1.74 |
| 0.5 | 0.03 | 1.28 | 0.10 | 1.26 | 1.13 | 2.01 |
| 0.6 | -0.02 | 1.25 | 0.02 | 1.21 | -0.67 | 1.93 |
| 0.7 | 0.01 | 1.22 | -0.05 | 1.17 | 0.02 | 1.55 |
| 0.8 | -0.05 | 1.17 | -0.06 | 1.14 | -0.34 | 1.39 |
| Averages | -0.09 | 1.22 | | 1.22 | -0.24 | 1.6 |

As seen the R1/R2 width estimate is compliant to both bias and standard deviation specifications. In general the standard deviation of the width is less than the velocity standard deviation for the same set of conditions. Subtle behavior is very similar to velocity in that standard deviation decreases with increasing SNR and increases with CSR with about the same fractional changes.

Table 18 - Doppler Data – Width (R1/R2); $N_S$ = 32, SNR = 30 dB
GMAP Performance - Blackman Window - System Noise as an Input

| | CSR= 10 dB | | CSR = 30 dB | | CSR = 50 dB | |
|---|---|---|---|---|---|---|
| $V/V_n$ | $W_{bias}$ ($ms^{-1}$) | SD[W] ($ms^{-1}$) | $W_{bias}$ ($ms^{-1}$) | SD[W] ($ms^{-1}$) | $W_{bias}$ ($ms^{-1}$) | SD[W] ($ms^{-1}$) |
| 0.0 | 0.40 | 0.80 | 0.88 | 0.78 | 1.15 | 0.75 |
| 0.1 | 0.32 | 1.07 | 0.46 | 1.15 | 1.02 | 0.94 |
| 0.2 | -0.29 | 0.99 | -0.70 | 1.02 | 0.80 | 1.26 |
| 0.3 | -0.38 | 0.96 | -0.67 | 0.94 | 0.91 | 1.45 |
| 0.4 | -0.05 | 1.10 | -0.21 | 1.10 | 1.15 | 1.69 |
| 0.5 | 0.09 | 1.22 | 0.09 | 1.23 | 1.10 | 1.88 |
| 0.6 | 0.01 | 1.11 | 0.11 | 1.18 | 0.64 | 1.77 |
| 0.7 | -0.01 | 1.01 | 0.03 | 1.05 | 0.08 | 1.34 |
| 0.8 | -0.06 | 1.10 | 0.09 | 1.07 | -0.16 | 1.21 |
| Averages | 0.0 | 1.04 | 0.01 | 1.06 | 0.74 | 1.37 |

Table 19 - Doppler Data – Width (R1/R2); $N_S$ = 64, SNR = 10 dB
GMAP Performance - Blackman Window - System Noise as an Input

| | CSR= 10 dB | | CSR = 30 dB | | CSR = 50 dB | |
|---|---|---|---|---|---|---|
| $V/V_n$ | $W_{bias}$ ($ms^{-1}$) | SD[W] ($ms^{-1}$) | $W_{bias}$ ($ms^{-1}$) | SD[W] ($ms^{-1}$) | $W_{bias}$ ($ms^{-1}$) | SD[W] ($ms^{-1}$) |
| 0.0 | -0.05 | 0.83 | 0.01 | 0.86 | 0.00 | 0.75 |
| 0.1 | -0.03 | 0.85 | 0.01 | 0.92 | 0.11 | 0.83 |
| 0.2 | -0.21 | 0.88 | -0.27 | 0.88 | 0.24 | 0.92 |
| 0.3 | -0.13 | 0.84 | -0.21 | 0.88 | 0.53 | 1.10 |
| 0.4 | -0.05 | 0.91 | 0.00 | 0.91 | 0.95 | 1.45 |
| 0.5 | -0.06 | 0.92 | -0.18 | 0.89 | 0.91 | 1.63 |
| 0.6 | -0.06 | 0.89 | -0.05 | 0.85 | 0.43 | 1.28 |
| 0.7 | -0.08 | 0.88 | -0.09 | 0.80 | -0.25 | 1.06 |
| 0.8 | -0.06 | 0.87 | -0.03 | 0.85 | -0.71 | 1.23 |
| Averages | -0.08 | 0.87 | -0.09 | 0.87 | 0.25 | 1.14 |

Table 20 - Doppler Data – Width (R1/R2); $N_S$ = 64, SNR = 30 dB
GMAP Performance - Blackman Window - System Noise as an Input

| | CSR= 10 dB | | CSR = 30 dB | | CSR = 50 dB | |
|---|---|---|---|---|---|---|
| $V/V_n$ | $W_{bias}$ ($ms^{-1}$) | SD[W] ($ms^{-1}$) | $W_{bias}$ ($ms^{-1}$) | SD[W] ($ms^{-1}$) | $W_{bias}$ ($ms^{-1}$) | SD[W] ($ms^{-1}$) |
| 0.0 | 0.10 | 0.71 | 0.27 | 0.70 | 0.13 | 0.60 |
| 0.1 | 0.12 | 0.80 | 0.19 | 0.80 | 0.20 | 0.72 |
| 0.2 | -0.20 | 0.75 | -0.27 | 0.78 | 0.31 | 0.80 |
| 0.3 | -0.26 | 0.80 | -0.29 | 0.83 | 0.58 | 1.05 |
| 0.4 | -0.09 | 0.86 | -0.88 | 0.96 | 0.98 | 1.42 |
| 0.5 | -0.02 | 0.88 | -0.02 | 0.85 | 1.01 | 1.63 |
| 0.6 | -0.01 | 0.78 | 0.01 | 0.78 | 0.27 | 1.15 |
| 0.7 | -0.01 | 0.77 | -0.05 | 0.79 | -0.25 | 0.94 |
| 0.8 | -0.07 | 0.78 | -0.11 | 0.77 | 0.64 | 1.14 |
| Averages | -0.06 | 0.79 | -0.13 | 0.81 | 0.43 | 1.05 |

The above Doppler mode spectrum width data was acquired using the R1/R2 estimator. Initially, all data was collected this way because the R0/R1 estimator had not been compensated for noise. Once SIGMET provided release 8.04.03, the team obtained additional simulations using the R0/R1 estimator. Results show there is not a significant difference in the GMAP performance of the two estimators at the benchmark condition.

## 12. GMAP Clear Air Mode Analysis

Clear Air data is acquired in one of two modes using either long pulse or short pulse. Long pulse mode, VCP 31, is about 9 dB more sensitive than short pulse, VCP 32. Both modes use volume acquisition schemes of redundant scans for reflectivity and Doppler data at low elevation angles and contiguous in VCP 31 and batch waveforms in VCP32 at the higher elevation angles.

Typical performance in VCP 31 is given in Tables 21, 22, and 23 with signal spectrum width of 2 $ms^{-1}$. Power estimate bias is generally less than 1 dB with typical value of about 0.5 dB. Estimate standard deviation as averaged over three 250 m cells to produce the 750 m sample volume depth estimate is less than 2 dB with typical values of about 1.3 dB. ( In so far as the three sample average represents a continuous average over the sample volume this average contains two independent samples [4]). As seen, the velocity and width is well within requirements with bias of a few tenths of a meter per second and standard deviation of less than 1 $ms^{-1}$ for velocity and 0.5 $ms^{-1}$ for width.

VCP 32 uses the short pulse PRT's i.e. same as VCP11 and 21. However, the number of samples is much larger, some 220 to 278 for PRT 5 through PRT 8. Performance is that given in Tables 11, 15, and 19 with a standard deviation reduction of about 1.85 for number of samples (220 and 64) and power estimate standard deviation increase of about 1.35 for spectrum width of 2 $ms^{-1}$ rather than 4 $ms^{-1}$ and velocity and width standard deviation decrease of about $\sqrt{2}$. Reduction factors are about 1.37 for power and 2.5 for velocity and spectrum width.

The parameters for Tables 21, 22 and 23 are:

SNR = 10 dB
$V_n$ = 12.08 $ms^{-1}$
$W_C$ = 0.28 $ms^{-1}$
$N_S$ = 64
$W_S$ = 2.0 $ms^{-1}$

Table 21 - Clear Air VCP 31 Reflectivity
GMAP Performance – Blackman Window – System Noise as an Input

| | CSR= 10 dB | | CSR = 30 dB | | CSR = 50 dB | |
|---|---|---|---|---|---|---|
| $V/V_n$ | $P_{bias}$ (dB) | SD[P] (dB) | $P_{bias}$ (dB) | SD[P] (dB) | $P_{bias}$ (dB) | SD[P] (dB) |
| 0.0 | -0.48 | 2.09 | -0.63 | 2.33 | -1.02 | 2.40 |
| 0.2 | -0.69 | 1.89 | -1.10 | 2.21 | -0.97 | 2.30 |
| 0.4 | -0.28 | 1.60 | -0.35 | 1.71 | -0.02 | 1.77 |
| 0.6 | -0.24 | 1.53 | -0.25 | 1.57 | -0.08 | 1.53 |
| 0.8 | -0.27 | 1.61 | -0.25 | 1.54 | -0.18 | 1.52 |
| 1.0 | -0.28 | 1.53 | -0.27 | 1.55 | -0.17 | 1.53 |
| Averages | -0.37 | 1.71 | -0.48 | 1.82 | -0.41 | 1.84 |
| Avg 750 m | | 1.21 | | 1.29 | | 1.29 |

Table 22 - Clear Air VCP 31 Velocity
GMAP Performance – Blackman Window – System Noise as an Input

| | CSR= 10 dB | | CSR = 30 dB | | CSR = 50 dB | |
|---|---|---|---|---|---|---|
| $V/V_n$ | $V_{bias}$ ($ms^{-1}$) | SD[V] ($ms^{-1}$) | $V_{bias}$ ($ms^{-1}$) | SD[V] ($ms^{-1}$) | $V_{bias}$ ($ms^{-1}$) | SD[V] ($ms^{-1}$) |
| 0.0 | 0.02 | 0.58 | 0.01 | 0.58 | 0.01 | 0.63 |
| 0.2 | 0.26 | 0.72 | 0.38 | 0.77 | 0.31 | 0.88 |
| 0.4 | 0.03 | 0.66 | 0.08 | 0.77 | -0.19 | 0.89 |
| 0.6 | 0.02 | 0.60 | 0.03 | 0.58 | -0.10 | 0.71 |
| 0.8 | 0.01 | 0.57 | 0.04 | 0.57 | -0.01 | 0.59 |
| Averages | 0.07 | 0.63 | 0.11 | 0.65 | 0.00 | 0.74 |

Table 23 - Clear Air VCP 31 Width
GMAP Performance – Blackman Window – System Noise as an Input

| | CSR= 10 dB | | CSR = 30 dB | | CSR = 50 dB | |
|---|---|---|---|---|---|---|
| $V/V_n$ | $W_{bias}$ ($ms^{-1}$) | SD[W] ($ms^{-1}$) | $W_{bias}$ ($ms^{-1}$) | SD[W] ($ms^{-1}$) | $W_{bias}$ ($ms^{-1}$) | SD[W] ($ms^{-1}$) |
| 0.0 | 0.03 | 0.43 | 0.08 | 0.39 | 0.19 | 0.39 |
| 0.2 | -0.09 | 0.47 | -0.17 | 0.48 | -0.08 | 0.52 |
| 0.4 | -0.08 | 0.47 | -0.08 | 0.48 | 0.08 | 0.56 |
| 0.6 | -0.01 | 0.45 | 0.01 | 0.47 | 0.02 | 0.53 |
| 0.8 | -0.06 | 0.43 | -0.03 | 0.45 | -0.07 | 0.40 |
| Averages | -0.04 | 0.45 | -0.04 | 0.45 | 0.03 | 0.48 |

## 13. Sensitivity of GMAP Performance to Clutter Spectrum Width and Filter Width

As noted earlier, there is only one input parameter for the GMAP filtering algorithm. It is the value of the expected clutter spectrum width. For all simulations presented so far, this input parameter has been set to 0.28 $ms^{-1}$. Per recommendation from SIGMET [10], the RVP8 GMAP filters were set based on the following parameters:

Using the RVP8 "Mf" menu, setup the clutter filters as follows:

Filter #1 - Type:3(GMAP) Spectrum width: 0.100 $ms^{-1}$
Filter #2 - Type:3(GMAP) Spectrum width: 0.150 $ms^{-1}$
Filter #3 - Type:3(GMAP) Spectrum width: 0.200 $ms^{-1}$
Filter #4 - Type:3(GMAP) Spectrum width: 0.250 $ms^{-1}$
Filter #5 - Type:3(GMAP) Spectrum width: 0.300 $ms^{-1}$
Filter #6 - Type:3(GMAP) Spectrum width: 0.350 $ms^{-1}$
Filter #7 - Type:3(GMAP) Spectrum width: 0.400 $ms^{-1}$

All simulations previously were conducted using Doppler filter number 5 which has an expected spectrum width of 0.30 $ms^{-1}$ which matches well with the simulation parameter of 0.28 $ms^{-1}$. Additional simulations were conducted to determine the

sensitivity of input clutter spectrum width. The following plots show the bias of reflectivity estimates as a function of CSR and the selected filter.

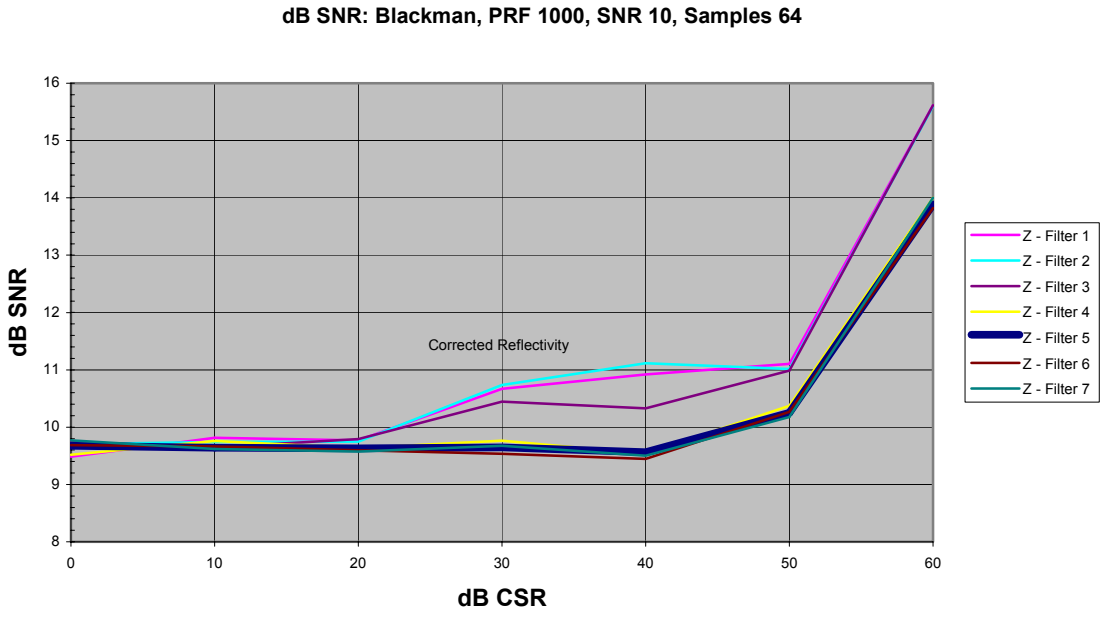


**Figure 25 - SNR Bias as a Function of Filter Width - Blackman Window**

Figure 25 shows performance of the reflectivity estimate as a function of CSR and selected Doppler filter. Here, filter # 5 is set for an expected clutter spectrum width of 0.3 $ms^{-1}$ which is close to the simulated clutter spectrum width of 0.28 $ms^{-1}$. Note that there is a measurable bias when filters 1 through 3 are used. These all are set for expected clutter widths less than the simulated signal clutter width. For filters 4 through 7, there is not much change in the bias performance. These filters are all set to values greater than or nearly equal to the simulated width.

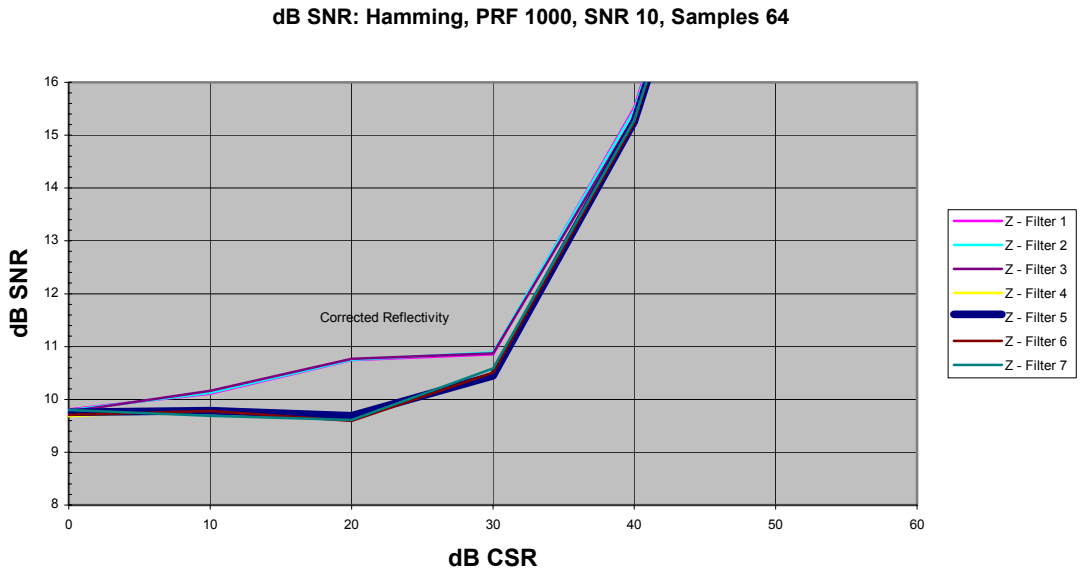


**Figure 26 - SNR Bias as a Function of Filter Width - Hamming Window**

Figure 26 shows the same analysis for the Hamming window data. Performance is similar to the Blackman window except that the data is acceptable only up to a little more than 30 dB as previously noted for the Hamming.

To complete the filter dependency analysis, additional runs were obtained for velocity and spectrum width performance as a function of selected filter and CSR in the same manner. Standard deviation performance is included. The next 10 figures present the data.

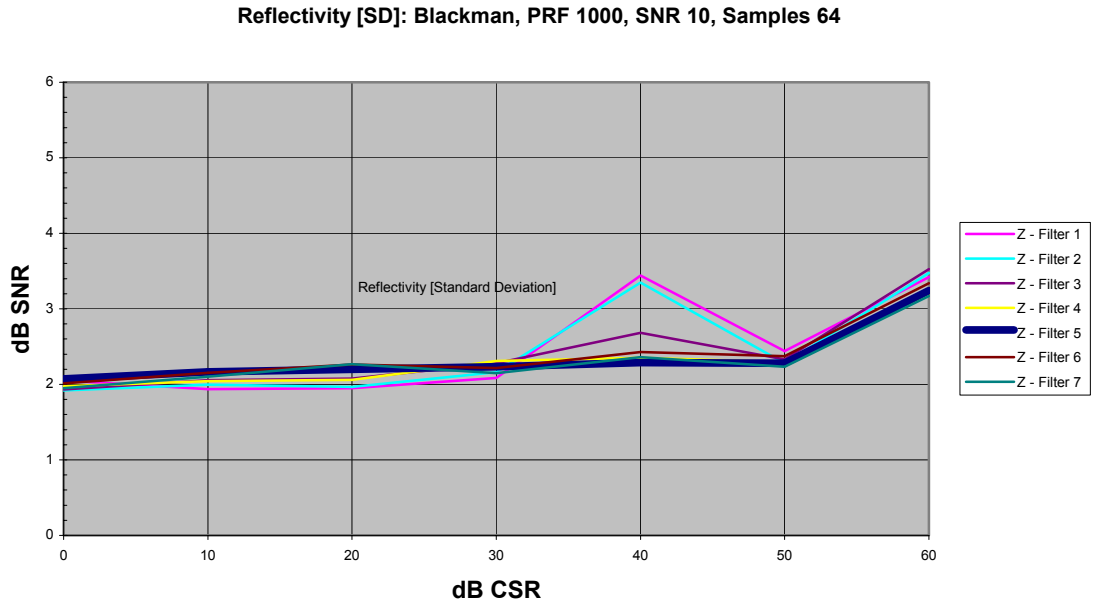


**Figure 27 - Reflectivity S. D. as a Function of Filter Width- Blackman**

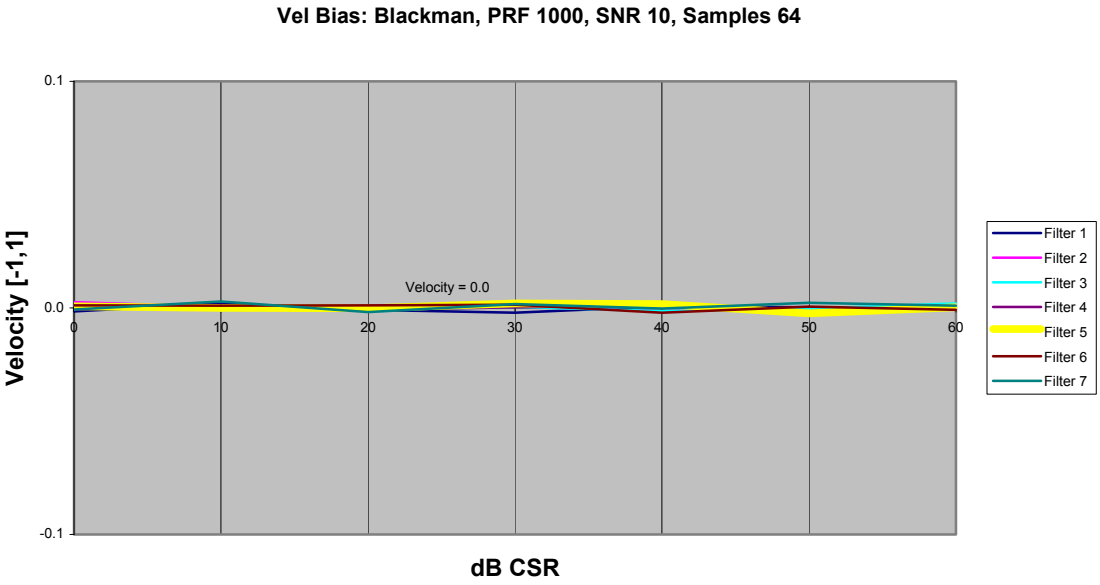


**Figure 28 - Velocity Bias as a Function of Filter Width - Blackman**

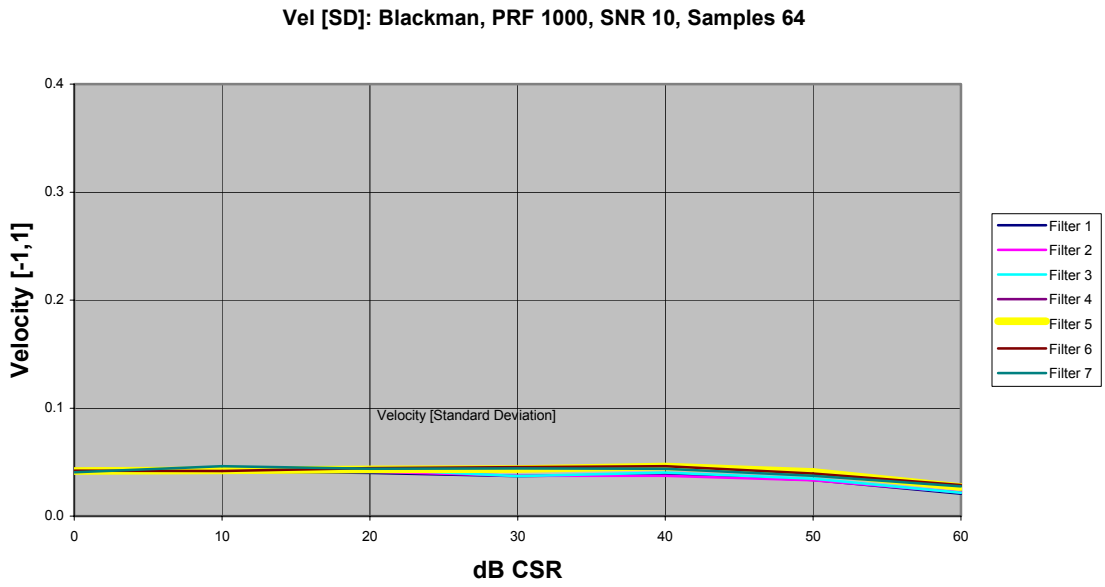


**Figure 29 - Velocity S.D. as a Function of Filter Width - Blackman**

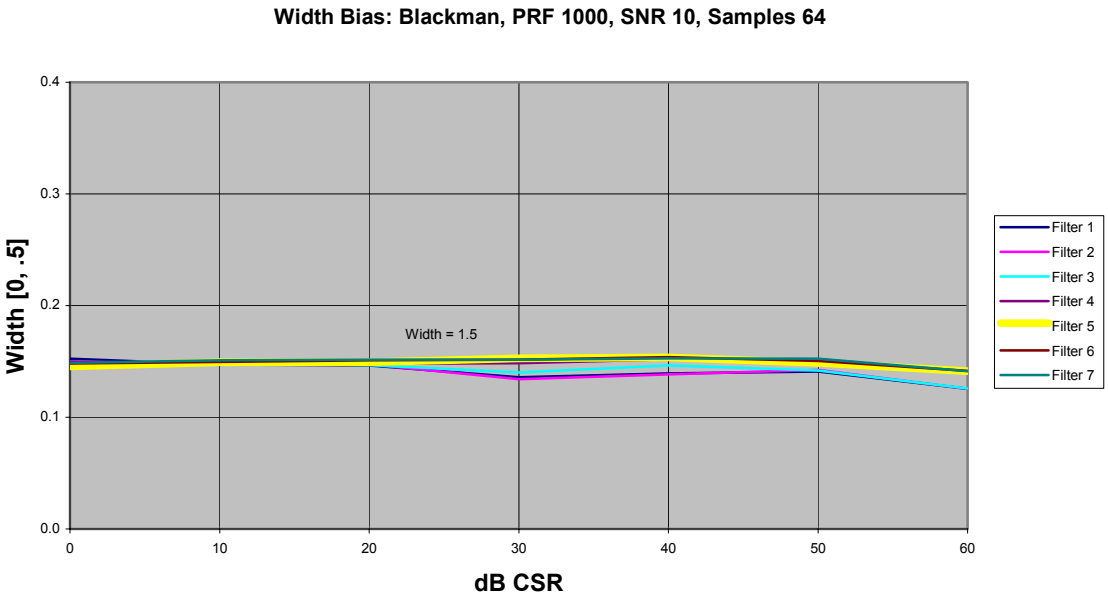


**Figure 30 - Width Bias as a Function of Filter Width - Blackman**

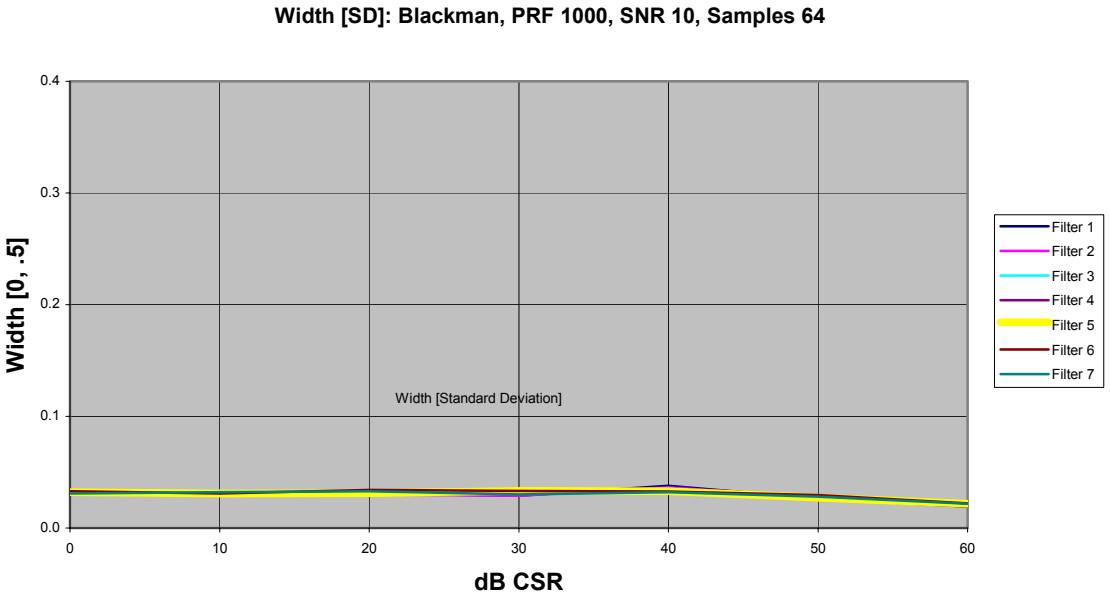


**Figure 31 - Width S.D. as a Function of Filter Width - Blackman**

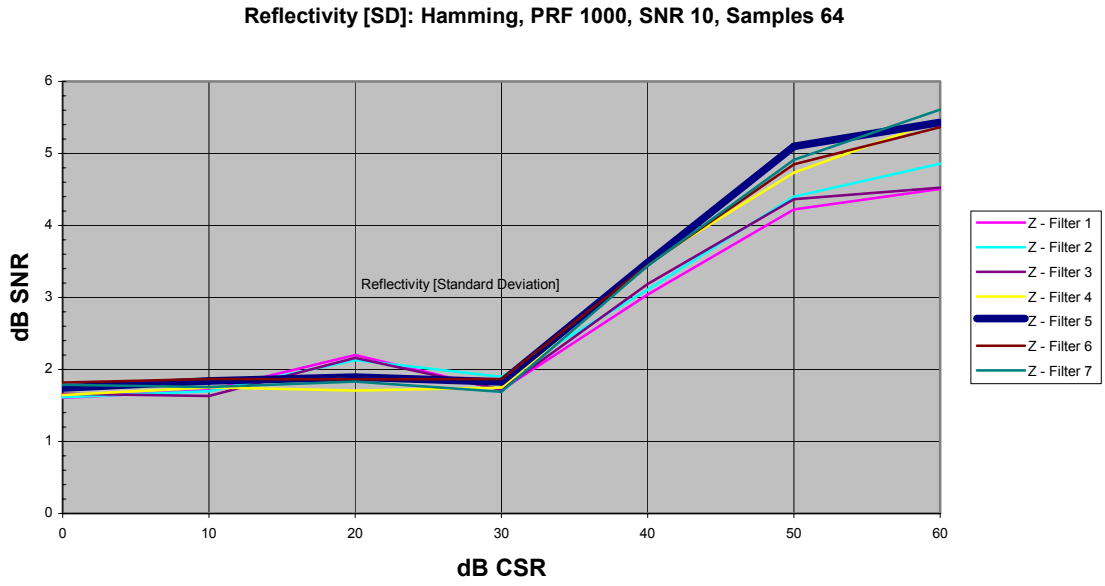


**Figure 32 - Reflectivity S.D. as a Function of Filter Width - Hamming**

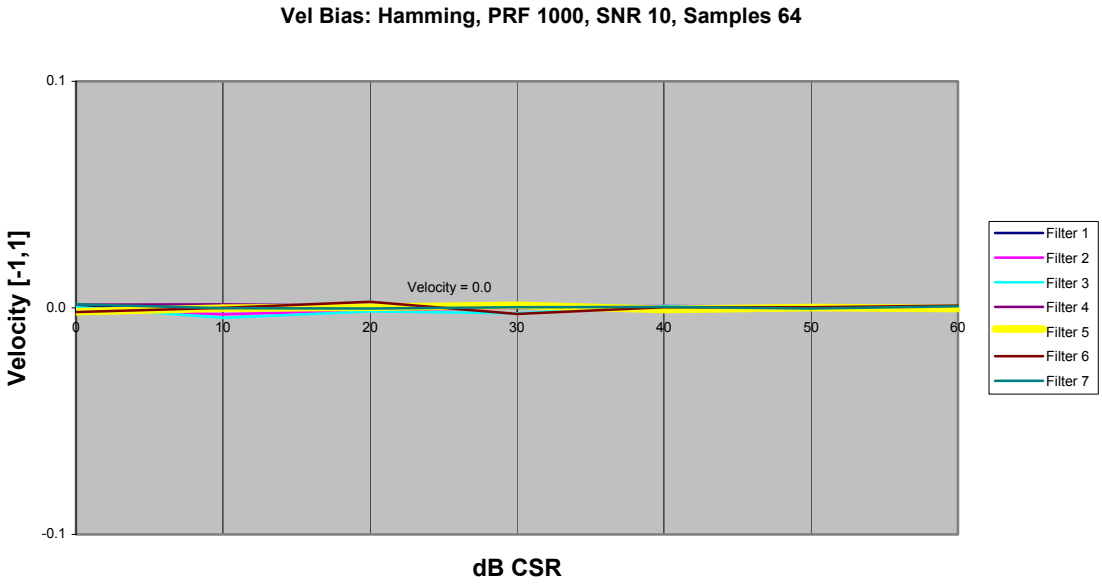


**Figure 33 - Velocity Bias as a Function of Filter Width - Hamming**

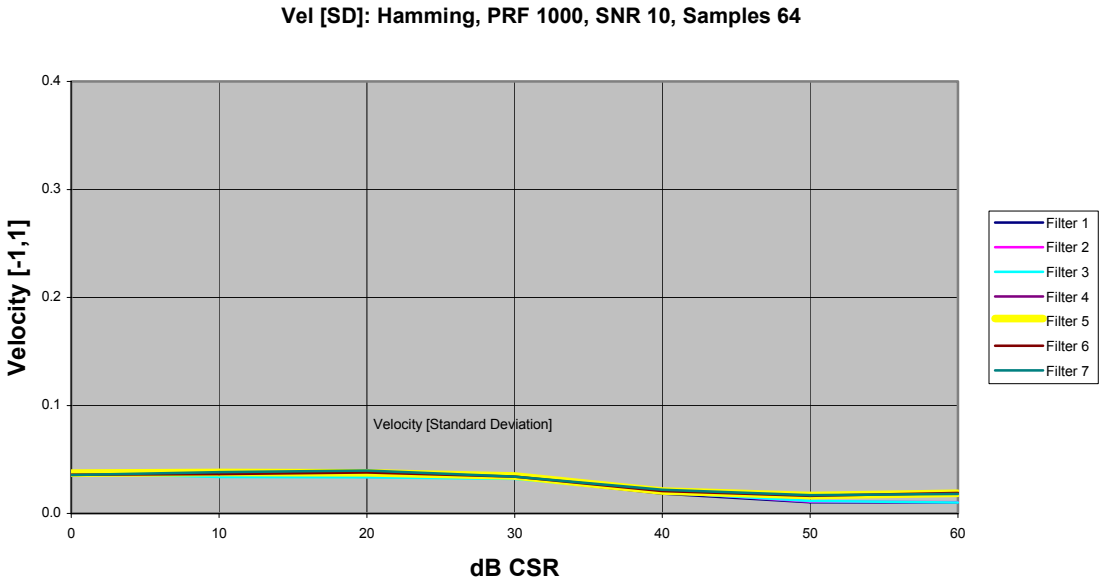


**Figure 34 - Velocity S.D. as a Function of Filter Width - Hamming**

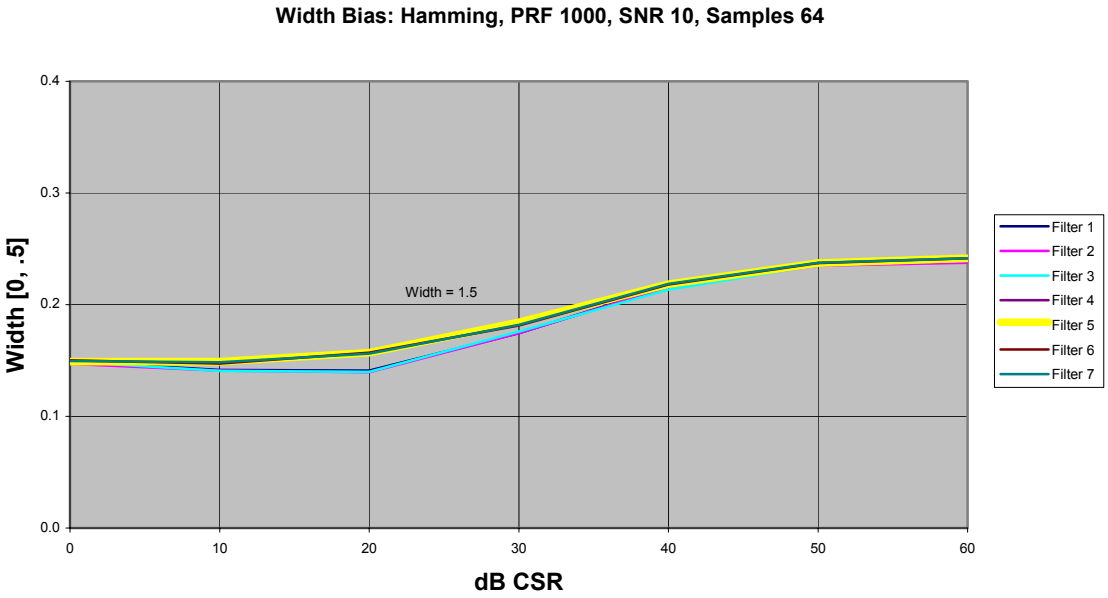


**Figure 35 - Width Bias as a Function of Filter Width - Hamming**

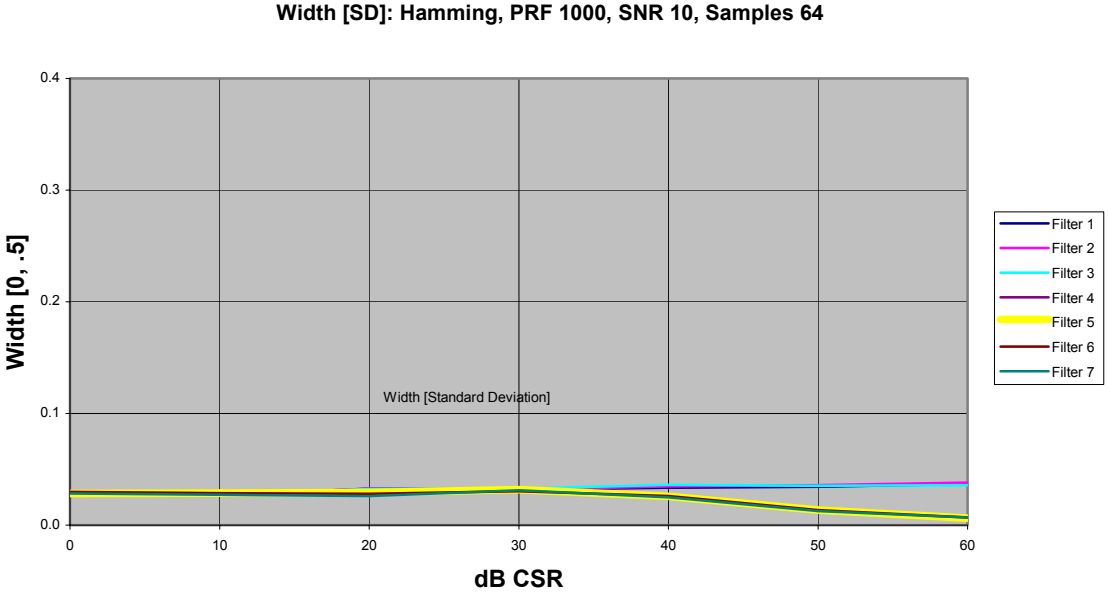


**Figure 36 - Width S.D. as a Function of Filter Width - Hamming**

## 14. Comparison of GMAP to Legacy Clutter Filters

The legacy Infinite Impulse Response (IIR) time domain filters are based on the concept of removing signal components within a designated band of frequencies. This is the traditional "notch" or high pass filter. There is a signal velocity value, the pass band edge velocity ($V_p$), that designates the point below which the signal is attenuated and above which it is allowed to pass without modification. In the WSR-88D legacy filters, the value of $V_p$ is changed, depending on the operating mode of the radar and the desired clutter suppression level. Once the filter is invoked, all signal components below, or near the pass band edge velocity are severely affected. The system does not distinguish between components due to clutter returns and those from weather echoes.

The ground clutter signal has zero mean velocity and spectrum width of a few tenths of a meter per second and thus is confined to the region around zero velocity. A high pass filter with stop band centered on zero frequency and stop band width comparable to the clutter signal width will remove most of the clutter signal. Again, the WSR-88D uses such a high pass filter for ground clutter suppression.

The particular filter design used is a 5-pole elliptic filter having a stop band depth of 60 dB, a pass band gain of 0.5 dB and pass band edge velocity ($V_p$) selectable from 0.5 $ms^{-1}$ to 4 $ms^{-1}$. Maximum clutter suppression achieved is slightly over 50 dB [8].

There are considerations in the use of a high pass filter. One is the signal spectral distortion which occurs when the signal is near zero velocity. That portion of the signal spectrum in the stop band is removed. This signal loss results in a reflectivity estimate bias as well as a velocity and width estimate bias due to spectrum distortion. The effects are minimized by choice of filter notch width.

As a result, notch width type filters induce a significant bias for weather signals with low velocity components such as those associated with slow moving storms, stratiform rain, and signals near the zero isotach. The amount of bias induced in reflectivity estimates can be anywhere from 4 dB to greater than 10 dB for narrow width, zero velocity mean signals, for surveillance reflectivity, and as high as 16 dB for Doppler reflectivity depending on established suppression level [8]. This reference documents the maximum bias in the reflectivity filters at ~ 10 dB for width = 1 $ms^{-1}$ and 2 dB for widths near 4 $ms^{-1}$. Maximum reflectivity bias for the Doppler mode filters is about 15 dB at 1 $ms^{-1}$ width and 2.5 dB for a width of 4 $ms^{-1}$. (This is also characteristic of the original 4-pole IIR filters supplied by SIGMET, but with higher bias, as much as 20 dB or more. [13].)

These characteristic biases for both the legacy 5-pole and the SIGMET 4-pole elliptic IIR filters are shown in the next figure, reproduced from [13]. The curves in Figure 37 show the reflectivity bias as a function of input signal spectrum width. The left plot is for surveillance mode filters and the ones on the right side are for Doppler mode filters. For the legacy filter, the three levels of selectable suppression are shown (low, medium, and high) and the pass band edge velocities are noted for legacy and for the SIGMET examples. As expected, the high suppression curves exhibit the highest bias while the low suppression ones have lowest bias. This analysis was conducted with zero mean velocity signals and the absence of a clutter signal in order to fully characterize the filter effects on meteorological signals. Note that the 4-pole SIGMET filters exhibit higher bias than the legacy 5-pole filters. This is expected since the 4-pole filters do not exhibit pass band edge roll off characteristics that are as sharp as the 5-pole filters. (The

elliptic filter is optimum in the sense that the transition from pass band to stop band is maximum for a given number of poles. The greater number of poles, the sharper the transition). For a given $V_p$, more of the signal components are affected by the 4-pole filters.

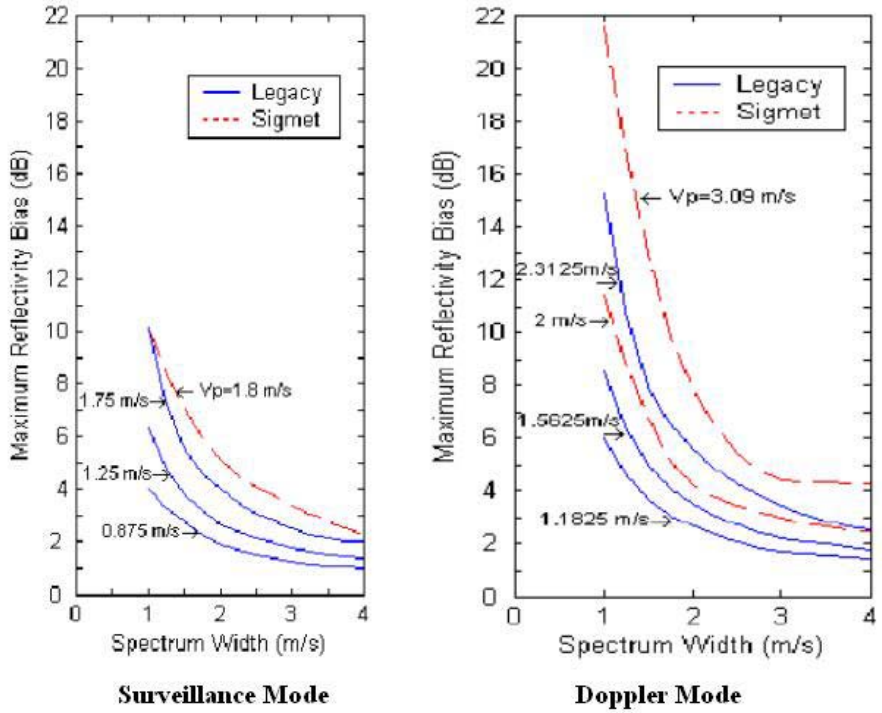


**Figure 37 - Legacy 5-Pole and SIGMET 4-Pole IIR Clutter Filter Reflectivity Bias**

Another consideration is filter response to rapidly varying input signals in azimuth (large reflectivity azimuthal gradients). As a multimode recursive device the filter has memory. This memory can result in data azimuthal "smearing" at low suppression and with antenna rotation rates greater than about 3 rpm [8]. This effect is again minimized by careful choice of notch width.

Other considerations are the filter performance constraints imposed by the WSR-88D data acquisition waveform. At intermediate antenna elevation angles the WSR-88D uses the batch waveform which breaks the time continuity of the input data stream. For good performance, the recursive filter must be initialized. However, even with initialization the suppression is less than that associated with a continuous data stream. Maximum suppression is reduced to about 33 dB. This is adequate for most radar sites, but limits use of the filter.

An adjunct consideration for radar systems evolution is the inherent phase distortion and inter-sample time spacing requirement of the recursive filter. It has been shown that recursive filters are not suitable for applications such as pulse to pulse staggered PRT and transmitter phase encoding [11].

The GMAP technique differs considerably from the WSR-88D legacy clutter filters. The GMAP filter does not have similar problems to the legacy because it is not a recursive filter. For example, the GMAP filter does not need to be initialized and suppression is not affected. Although not yet tested, the GMAP filter should be suitable for phase coding applications and some staggered PRT techniques. The GMAP technique also has the potential to produce lower bias effects on weather signals since it is not simply a component removal process as is the case for a notch filter. GMAP attempts to not only remove clutter component coefficients, but restores signal components within the affected regions using a Gaussian model. As described in section 8, the GMAP algorithm is a spectral component removal and reconstruction process. The scheme assumes the presence of clutter having a width provided by the filter selected i.e. the command from the clutter map.

The team evaluated performance of GMAP when supplied only with a weather signal, absent clutter. This was done for weather signals having zero mean widths and relatively narrow spectra. This represents the worst case for evaluating the effects of filtering on weather signals near the zero isotach. A similar analysis is available for the legacy filter performance [8]. Processing of the weather signal alone is realistic in practice since the clutter map could contain errors due to false detection in map generation or the clutter target may longer exist in that region. A limited number of map errors will probably occur. Therefore it is useful to analyze filter effects on weather signals alone. This is particularly important for weather signals at the zero isotach with narrow widths.

Additional simulations using GMAP with variable spectrum widths were obtained for comparison with legacy performance. The next three figures show the GMAP reflectivity estimate bias performance for a zero velocity signal as a function of spectrum width in the absence of clutter, although the GMAP has received a clutter process and clutter width command. This would be the case where an error occurred in map generation or when a clutter signal has faded away (as with anomalous propagation). All three weather modes are shown. Figure 38 displays the effect GMAP has on a weather signal of 20 dB as spectrum width is varied between 1 and 4 $ms^{-1}$. An SNR of 20 dB is referenced in the WSR-88D specifications and is also a signal level commonly observed in a recent spectrum width study [14]. This level was chosen to more closely repeat the data of Figure 37.

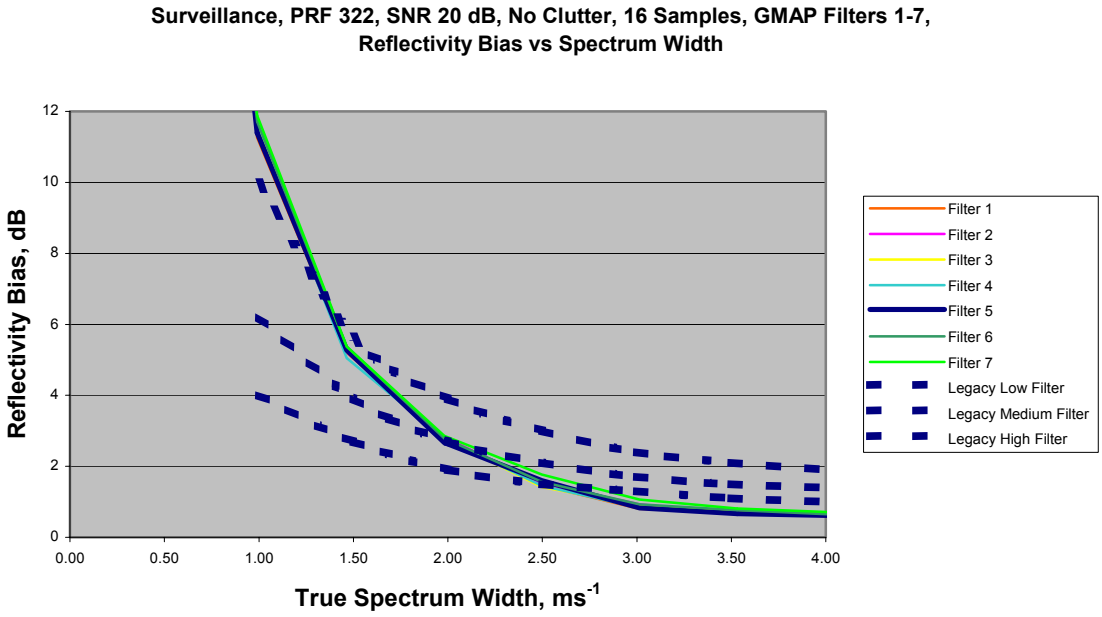


**Figure 38 – GMAP Reflectivity Bias – Surveillance – No Clutter**

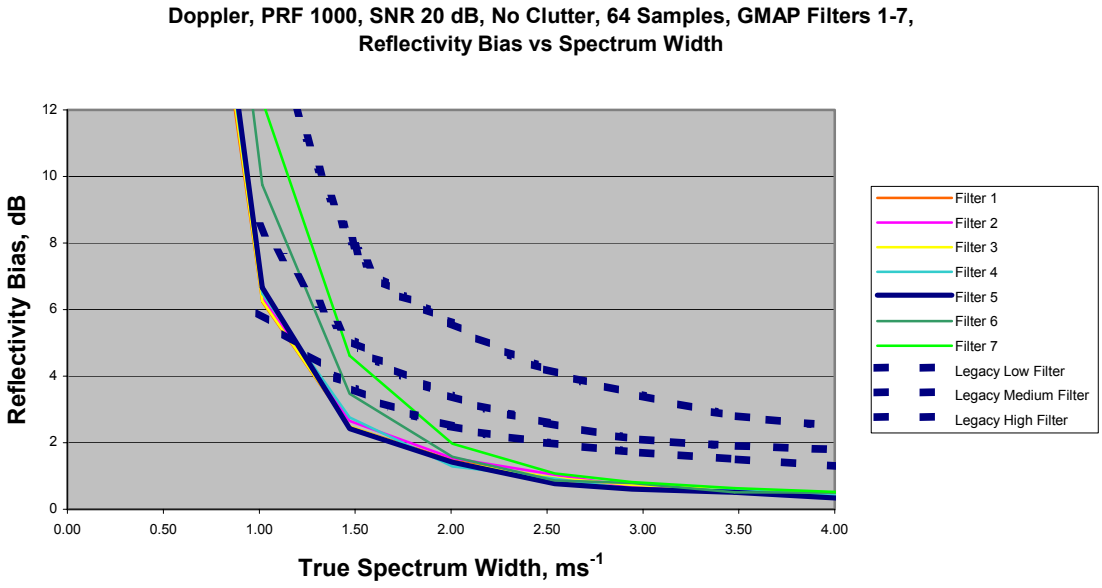


**Figure 39 – GMAP Reflectivity Bias – Doppler – No Clutter**

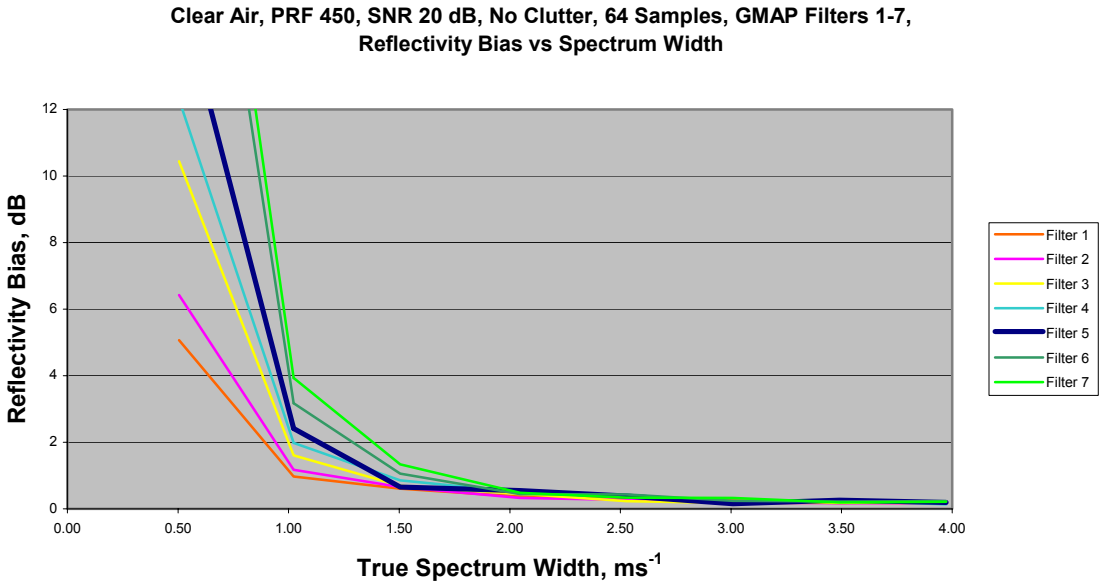


**Figure 40 – Reflectivity Bias – Clear Air – No Clutter**

For all three weather modes (Surveillance, Doppler, and Clear Air), the reflectivity bias is significantly lower than the bias associated with the legacy filters over much of the input spectrum width range. The effects of selecting variable GMAP filter widths is also featured in the figures, with filter #5 again matched to the expected input clutter spectrum width.

The GMAP performance should be compared to the maximum suppression legacy filter because this is the filter necessary to deliver the maximum suppression of 55 dB which equates to the GMAP performance. With this in mind, it can be seen from Figure 38 that for the Surveillance mode, the GMAP process exhibits less bias than the legacy for mean input signal spectrum widths down to 1.5 $ms^{-1}$. Performance is equivalent for lower widths. Bias performance for the Doppler and Clear Air modes is better than with the Surveillance mode with Clear Air exhibiting the best performance.

Although not displayed, it was found that as the velocity is moved away from the zero isotach the overall reflectivity bias decreased across the range of narrow spectrum widths (0.5 to 4 $ms^{-1}$). Thus by selecting zero velocity, the worse case for bias performance is exhibited. Also note that filter selection does not appear to have an appreciable effect on the bias performance at zero velocity for narrow spectrum widths.

The next six figures summarize bias performance for velocity and spectrum width in all three weather modes with the same input parameters as above. The bias performance is good with the exception of the spectrum width estimate for the Doppler mode and very narrow widths. This data was generated using the R0/R1 estimator which performs slightly worse than the R1/R2 estimator at these low widths.

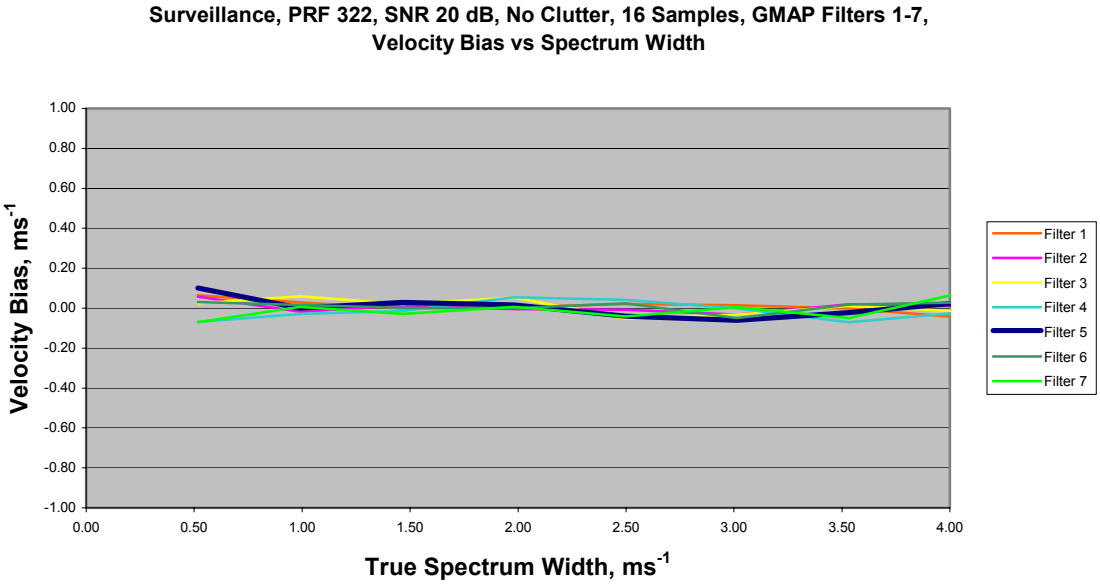


**Figure 41 – GMAP Velocity Bias – Surveillance – No Clutter**

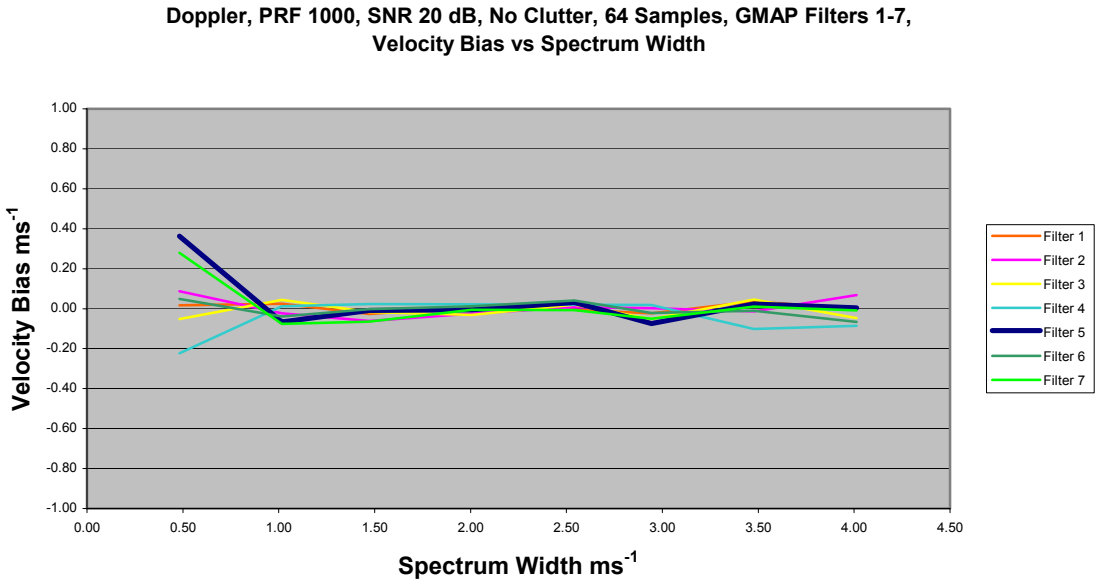


**Figure 42 – GMAP Velocity Bias – Doppler – No Clutter**

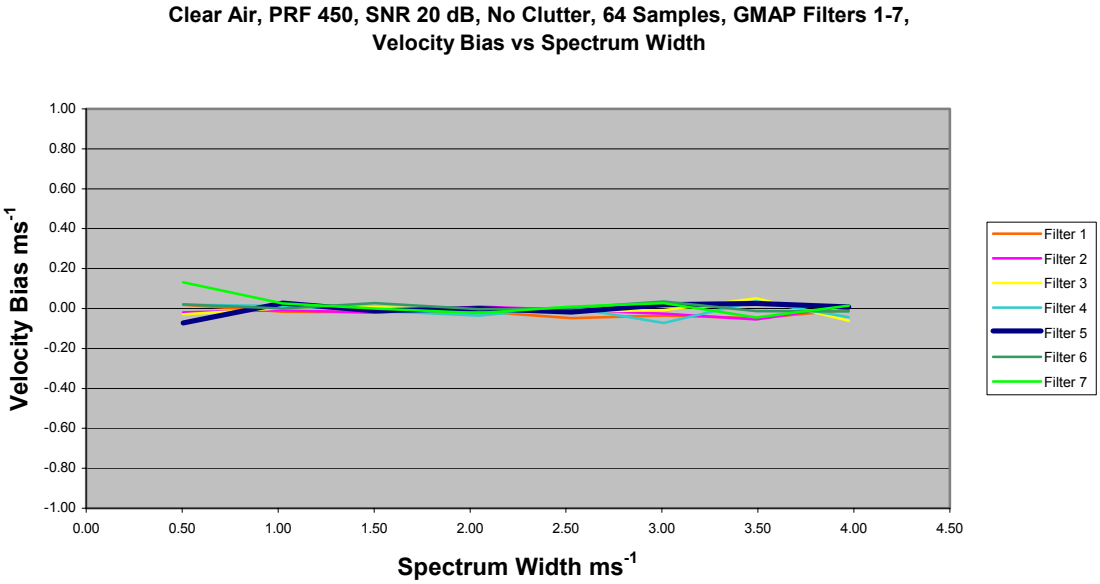


**Figure 43 – GMAP Velocity Bias – Clear Air – No Clutter**

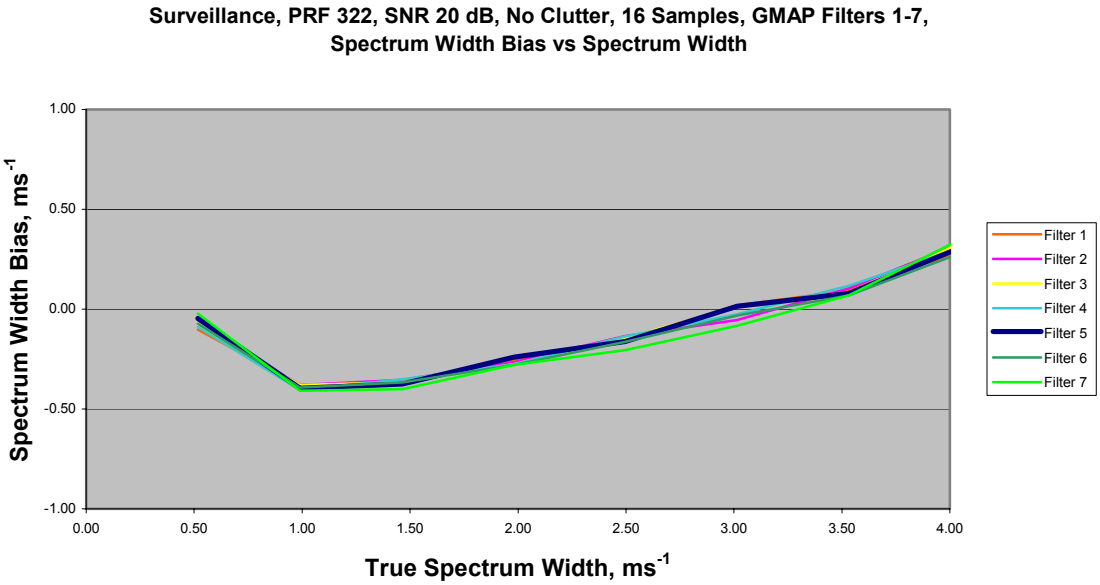


**Figure 44 – GMAP Spectrum Width Bias – Surveillance – No Clutter**

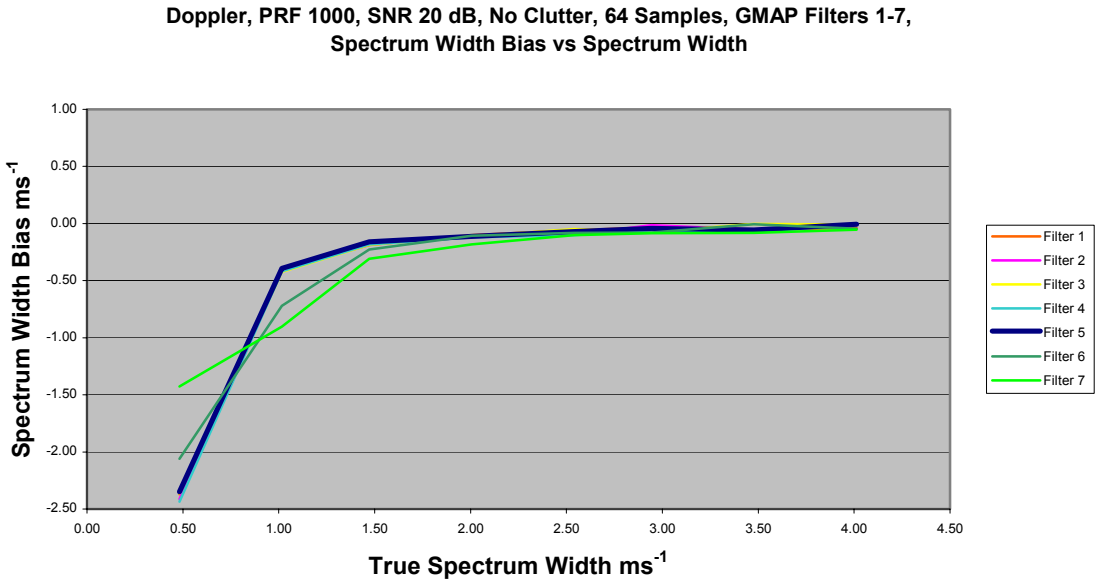


**Figure 45 – GMAP Spectrum Width Bias – Doppler – No Clutter**

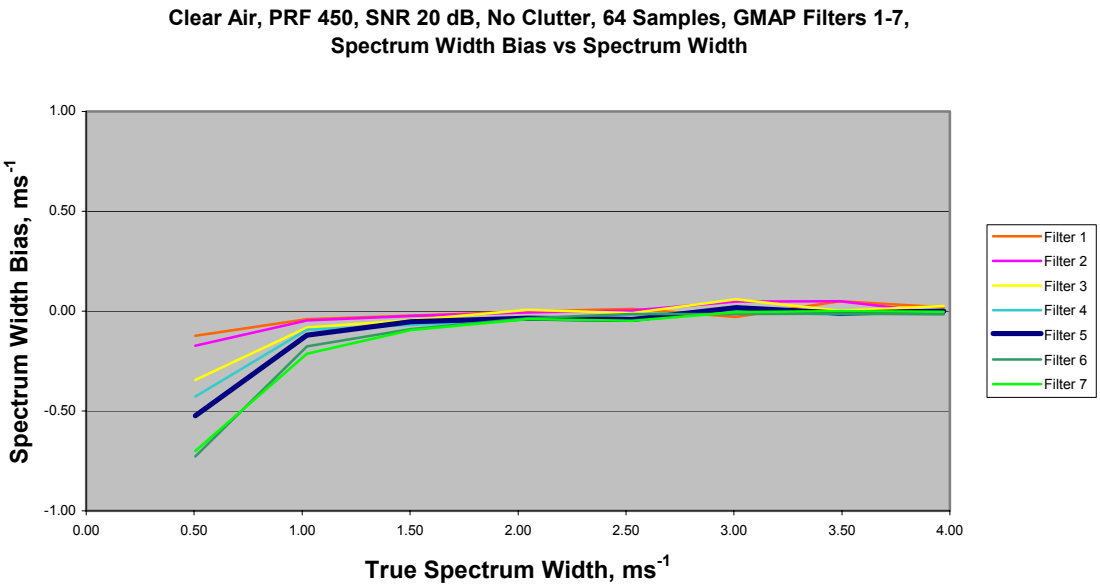


**Figure 46 – GMAP Spectrum Width Bias – Clear Air – No Clutter**

In summary, GMAP operating on signal alone results in a reflectivity bias along the zero isotach. This bias ranges from a level of about one half to one third that of the legacy high suppression filter at large spectrum widths to a bias roughly equal to the that of the high suppression filter at narrow widths. Performance is generally comparable to the legacy filter. This accents the obvious need for careful clutter map generation to minimize map errors.

In normal operation on a mix of signal and clutter the GMAP delivers essentially unbiased estimates of all three spectral moments (sections 10 ,11, and 12) as compared to the recursive filter which induces reflectivity bias greater than 10 dB typically. GMAP has little spectral distortion compared to the notch filter. There is no azimuthal "smearing" with the GMAP since the scheme relies on data block processing and does not consider samples outside the radial being processed. The scheme is not constrained

by the batch waveform or other data acquisition waveforms so long as there are adequate samples for analysis.

Although yet to be demonstrated, it appears that GMAP will adapt to the radar signal phase coding schemes. The suitability of GMAP for the intra pulse staggered PRT scheme (pulse to pulse PRT change) is unknown at this time and requires further investigation. GMAP will accommodate any type of batch PRT scheme as long as an adequate number of pulses are available.

The major advantage of GMAP compared to the legacy filter is recovery of quantitative data on and near the zero isotach. The major disadvantage is an increase in variance of the spectral moment estimates.

**15. GMAP Performance at Low SNR and Clutter Levels**

Additional simulations were completed in order to obtain data potentially useful for designing the clutter map generation process and to explore GMAP performance at lower SNR's and clutter levels and small signal spectrum widths. This data was obtained for SNR's of 3 and 8 dB with CSR's of 0, 3, and 10 dB.

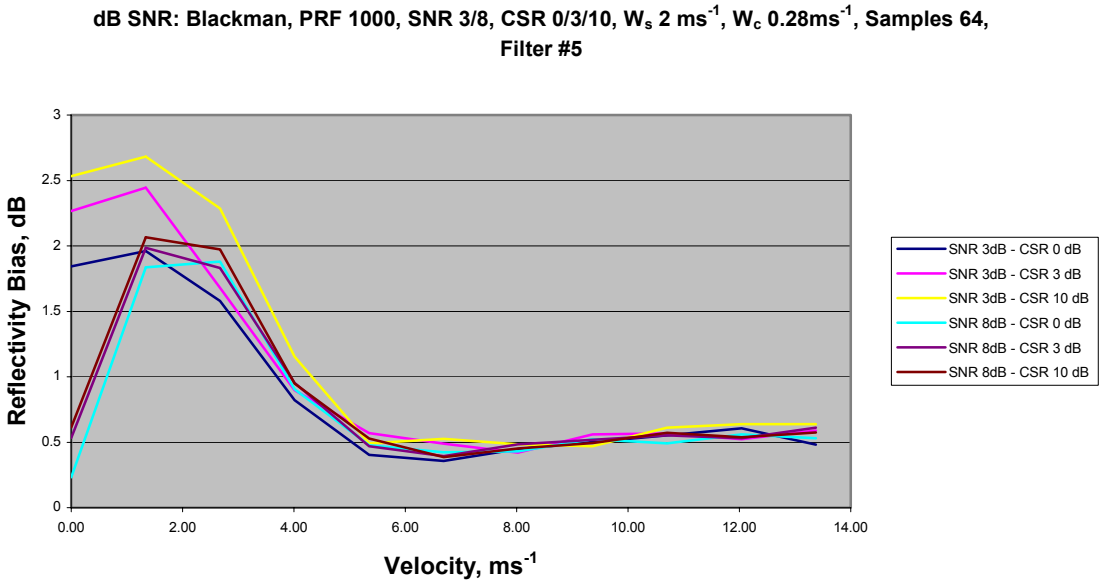


**Figure 47 - Low SNR Reflectivity Bias**

The data was generated for a PRF of 1000 Hz and 64 samples. Figure 47 is the reflectivity estimate bias as a function of velocity for a weather signal of 2 $ms^{-1}$. Doppler filter # 5 is selected to match with the specified clutter spectrum width of 0.28 $ms^{-1}$. All cases of both SNR's and the three CSR's are depicted. A constant bias of around 0.5 dB is noted for input velocities greater than about 5 $ms^{-1}$ with a maximum bias of about 2.7 dB for the 3 dB SNR, 10 dB CSR case at an input velocity of just under 2 $ms^{-1}$.

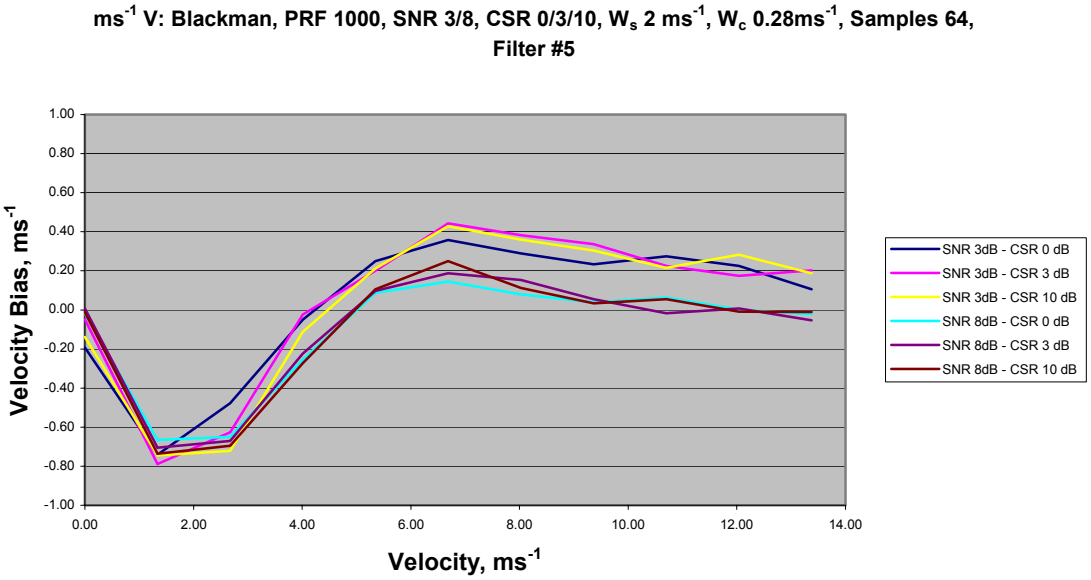


**Figure 48 - Low SNR Velocity Bias**

Figure 48 shows the velocity bias for the same input conditions. The bias ranges from around – 0.7 $ms^{-1}$ for low input velocities to a maximum positive bias of about 0.4 $ms^{-1}$ at just over 6 $ms^{-1}$ mean input velocity. Above a mean input velocity of 4.5 $ms^{-1}$, the higher SNR signals exhibit less bias than the lower SNR group. Below about 3 $ms^{-1}$ mean input velocity, there is not much difference in bias performance.

Figure 49 is the spectrum width estimator bias. The bias for the 8 dB SNR cases is always more positive than that of the 3 dB SNR cases. For the 8 dB SNR data, biases range from near zero to a maximum of 0.4 $ms^{-1}$, averaging to about 0.2 $ms^{-1}$ for sufficiently large velocities (> 6 $ms^{-1}$). For SNR of 3 dB, the bias ranges from as much as –0.8 $ms^{-1}$ to about –0.1 $ms^{-1}$, averaging around –0.3 $ms^{-1}$ for velocities larger than about 6 $ms^{-1}$.

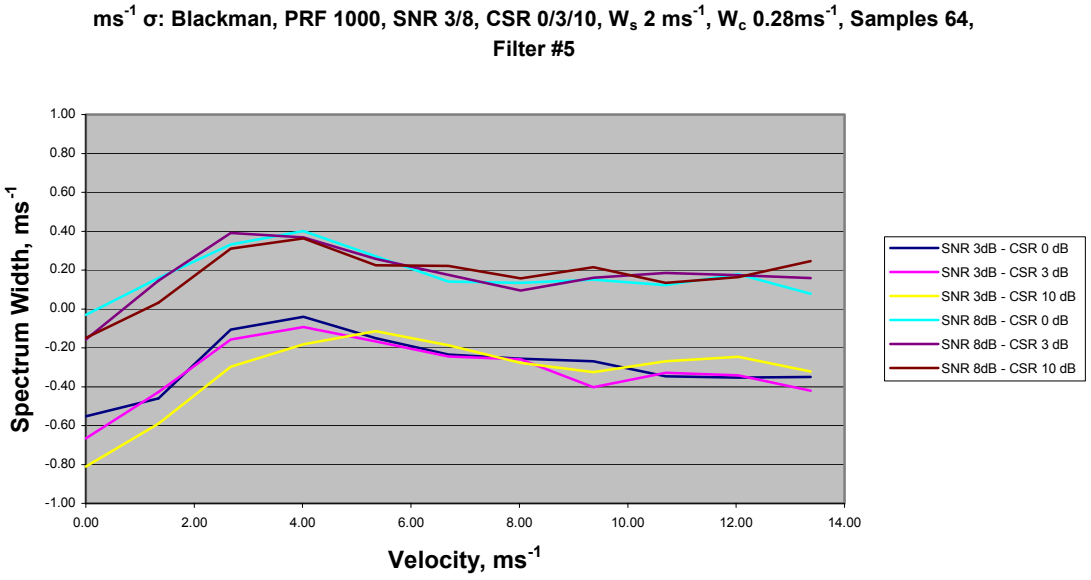


**Figure 49 - Low SNR Spectrum Width Bias**

Bias performance for these low SNR's, at least for this Doppler mode PRF (1000 Hz) and associated sample number (64) is well within system specifications (except for reflectivity bias for a small region of low input velocities and low SNR). Regarding clutter map generation, note that the magnitude of the time domain moment estimator biases, particularly the bias of both width estimators for very narrow spectra, precludes the use of the real time process methods for clutter map generation. Accurate clutter map generation will require use of spectral techniques for estimating clutter spectrum width.

## 16. Conclusions

The evaluation team offers the following conclusions regarding the spectrum width estimators and GMAP, based the simulation experience.

Spectrum Width Estimators

R0/R1 Estimator

The R0/R1 estimator without noise compensation meets WSR-88D bias requirements for signal to noise ratios greater than 30 dB over true spectrum widths from 0.5 $ms^{-1}$ to at least 8.0 $ms^{-1}$.

The R0/R1 estimator without noise compensation meets WSR-88D standard deviation requirements for signal to noise ratios greater than 20 dB over true spectrum widths from 0.5 $ms^{-1}$ to at least 8.0 $ms^{-1}$.

The R0/R1 estimator with system noise as an input (Release 8.04) meets WSR-88D bias requirements for signal to noise ratios greater than 20 dB over true spectrum widths from 0.5 $ms^{-1}$ to at least 8.0 $ms^{-1}$.

The R0/R1 estimator with noise compensation (Release 8.04.03) meets WSR-88D standard deviation requirements for signal to noise ratios greater than 10 dB over true spectrum widths from 0.5 $ms^{-1}$ to at least 8.0 $ms^{-1}$.

The R0/R1 estimator with noise compensation exhibits less bias than the R1/R2 estimator for true spectrum widths greater than about 4 $ms^{-1}$.

R1/R2 Estimator

The R1/R2 estimator meets WSR-88D specifications (< 1 $ms^{-1}$ bias and standard deviation) at the benchmark (10 dB SNR, W = 4 $ms^{-1}$)

The R1/R2 estimator meets WSR-88D bias and standard deviation requirements for signal to noise ratios greater than 10 dB over true spectrum widths from 0.5 $ms^{-1}$ to at least 6.5 $ms^{-1}$.

The R1/R2 estimator exhibits slightly greater bias (negative bias) than the R0/R1 estimator (with noise compensation) for true spectrum widths greater than about 4 $ms^{-1}$.

## GMAP Clutter Filtering Technique

### General Observations

The GMAP technique is not based on the concept of a high pass (notch width) filter.

Thus, the GMAP technique does not require filter initialization, does not exhibit the azimuthal smearing seen in the legacy filters, and does not result in large reflectivity and velocity bias near and on the zero isotach.

The GMAP technique can recover a signal at any clutter to noise ratio so long as the signal is no more than 55 dB below the clutter.

The GMAP technique delivers unbiased reflectivity, velocity, and spectrum width estimates over a larger range of signal velocity, signal to noise ratios, and clutter to signal ratios than the legacy 5 pole elliptic filters.

The GMAP technique should be applicable to both phase coding and may also be applicable to staggered PRT range velocity ambiguity mitigation enhancements.

### GMAP With Rank Order Noise Estimation

The GMAP technique using the rank order noise estimate is immune to potential system noise measurement errors.

The GMAP technique with the rank order noise estimate feature meets WSR-88D requirements for all Doppler and Clear Air Modes (estimator input samples greater than N = 32)

The GMAP technique with the rank order noise estimate feature does not meet WSR-88D requirements for the Severe Weather (Convective) Surveillance Mode (estimator input samples N = 16).

GMAP with System Noise Value Input

The GMAP technique using the system noise value as an input meets WSR-88D requirements for most Severe Weather and Clear Air Modes (estimator input samples $N \geq 16$). Note that this observation is dependant on accurate system noise measurement.

GMAP Window Functions

GMAP with the Blackman window function meets WSR-88D requirements for Clutter to Signal ratios of up to 55 dB.

GMAP with the Hamming window function meets WSR-88D requirements for Clutter to Signal ratios of up to 33 dB.

GMAP with the Hamming window function delivers a slightly lower standard deviation of the estimate as long as Clutter to Signal ratios are less than 33 dB.

The GMAP Adaptive window selection feature, selecting between Hamming and Blackman windows only, does not offer a significant performance advantage over simple selection of the Blackman window at the present stage of development.

There is potential for improvement with advanced window selection designs, possibly including features with additional windows and selection of the rectangular window when no clutter is present.

GMAP Filter Widths Matched to Clutter Spectrum Width

The performance of the GMAP filter depends on matching filter width to the expected spectrum width of the clutter. This will likely require frequent and accurate clutter map generation which includes a measurement of clutter spectrum width in each cell.

Analysis indicates that for cases where the clutter spectrum width is not exactly matched to the filter width, GMAP performs better if the GMAP filter width is wider than the clutter spectrum width.

## 17. Recommendations

The evaluation team offers the following suggestions for NEXRAD program management regarding spectrum width estimators and implementation of the GMAP clutter filter method.

An adaptive spectrum width estimator selection process is recommended for the WSR-88D. The process should select outputs from either the R0/R1 or the R1/R2 (lag 2 or poly pulse) estimator using signal to noise ratio and true spectrum width as selection criteria.

If only one spectrum width estimator is used initially, it should be the R0/R1 estimator because it exhibits a more linear bias and better variance over a wider range of input spectrum widths.

For good performance of the R0/R1 spectrum width estimator, the ORDA design should ensure accurate system noise measurements or estimation. This may be an

adaptive process selecting between the rank order noise estimate and use of measured system noise values.

The GMAP Clutter Filter technique is recommended for the ORDA.

Implementation of GMAP requires development of a new clutter map generation process which includes measurements of clutter spectrum width. This process should be designed to be easy to perform with minimal operational impact.

Improved adaptive window selection for GMAP should also be considered as part of a future enhancement to the ORDA.

## 18. Future Work

The evaluation team recommends the following actions continue in support of the ORDA project and future enhancement developments.

The team should conduct the next phase of evaluation which is based on actual radar data rather than simulations (part 2 of this study). This can include the use of legacy archived time series data as well as time series and moment products from other radar sources. Potential sources include the extensive data base generated by the Joint Polarization Experiment (JPOLE) project.

The performance of GMAP with Phase Coding needs to be extensively examined. Both of these techniques are computationally intense, using multiple Fourier Transform operations. The two processes need to be efficiently integrated for practical implementation in the RVP8.

The applicability of GMAP to Staggered PRT techniques requires further examination. The evaluation team should work closely with the R-V Ambiguity Mitigation project to determine if a form of GMAP can be designed to support intra-pulse staggered PRT.

The evaluation team should continue to evaluate issues related to implementing new science techniques into the ORDA RVP8 system. These include over sampling, full power spectrum analysis, and increased product resolution.

## 19. Acknowledgements

The evaluation team would like to recognize several individuals for their support to this effort. Nita Patel of the RSIS ORDA team provided expert advice and guidance as well as access to an ORDA team RCP8/RVP8 asset. Rick Rhoton of the ROC/RSIS team provided considerable assistance with system configuration and advice on operating the SIGMET software. Alan Siggia and Richard Passarelli of SIGMET provided valuable technical advice as well as rapid software updates which helped keep the project on schedule. Lt Ron Fehlen, Radar Engineering Team Leader, provided excellent guidance and support for this project.

## 20. References

[1] “Numerical Comparison of Five Mean Frequency Estimators”, D. Sirmans and B. Bumgarner, Journal of Applied Meteorology, Vol 14, No. 6, September, 1975.

[2] NEXRAD Technical Requirements

[3] “On the Use of Windows for Harmonic Analysis with the Discrete Fourier Transform”, F. J. Harris, Proceedings of the IEEE, Vol. 66, No. 1, January 1978.

[4] Sirmans, D. and R. J. Doviak, 1973; Meteorological Radar Signal Intensity Estimation, NOAA Technical Memo ERL NSSL-64, National Severe Storms Laboratory, Norman, OK 80 pp [NTIS COM-73-11923/2AS]

[5] Zrnic, D. S., 1977; Spectrum Moment Estimates from Correlated Pulse Pairs; IEEE Transactions of Aerospace Electronic Systems, AES-13, 344-354.

[6] Doviak, R. J. and Zrnic, D. S.; Doppler Radar and Weather Observations, 2nd Edition, Academic Press, 1993.

[7] Siggia, A., Oct 2003, Private Communication from SIGMET, Inc.

[8] Sirmans, D.; 1992; Clutter Filtering in the WSR-88D, Operational Support Facility Internal Report.

[9] Sirmans, D.; Note on Spectrum Width Calculation in the WSR-88D and Recommended Software Changes, WSR-88D Operational Support Facility, Internal Report, February 1998.

[10] Siggia, A., September 13, 2003, Private Communication

[11] Zrnic, D., Torres, S., Dubel, Y., Keeler, J., Hubbert, J., Dixon, M., Meymaris, G., Ellis, S., National Center for Atmospheric Research and National Severe Storms Laboratory, FY 2003 NCAR-NSSL Interim Report, "NEXRAD Range-Velocity Ambiguity Mitigation SZ(8/64) Phase Coding Algorithm Recommendations" August 15, 2003.

[12] Torres, S., "Estimation of Doppler and Polarimetric Variables for Weather Radars", PhD Dissertation, University of Oklahoma, 2001.

[13] Sirmans, D., Patel, N., Leatherman, R., "ORDA Clutter Filtering Options Assement and Recommendation", Office of Science and Technology, Open RDA Project, Internal Report, January 2003.

[14] Fang, M., Doviak, R., "Spectrum Width Statistics of Various Weather Phenomena" National Severe Storms Laboratory, Internal Report, September 2001.